OES and CARS on an expanding argon/hydrogen plasma jet

Box, C.

Award date:
1997

OES and CARS on an expanding argon/hydrogen plasma jet

Graduation report of
Marco Box

December 1994 VDF/NT 94-23

Supervisors:
Ralph Meulenbroeks
Richard Engeln
Daan Schram
Joost van der Mullen

Eindhoven University of Technology
Department of Physics

Summary

The work described in this report can be divided in two parts:

1 An expanding plasma jet is investigated by means of optical emission spectroscopy. The aim of the experiments was to obtain information about the hydrogen kinetics in the region in front of the stationary shock. The production mechanisms of excited hydrogen atoms were studied. The main sources of excited atomic hydrogen proved to be three particle recombination and dissociative recombination of ArH^+ after associative charge exchange of argon ions with hydrogen molecules.
When burning the cascaded arc on a mixture of argon and hydrogen gas the observed densities of excited hydrogen atoms at the center of the plasma near the nozzle could be explained totally by three particle recombination. The effects of changes inside the arc (deteriorating efficiency, shift from ionisation of argon to hydrogen) appear to heavily influence the densities of charged and excited particles in the expansion.
Since earlier experiments indicated a recirculation flow of molecular hydrogen near the vessel wall, which causes transport of H_2 to the plasma to occur, a second experiment was performed in order to gain further proof of this indication. In this case the H_2 gas was admixed to the plasma outside the arc. Under this condition only dissociative recombination can explain the observed population of excited hydrogen atoms.
It was now found that in order to be able to explain the densities of excited hydrogen atoms rovibrationally excited hydrogen molecules, coming from the vessel wall, must be present in the plasma.

2 The CARS diagnostic has been carefully tested and a computer program was written in order to be able to perform automatic experiments. The computer program is able to accurately position the tunable dye laser at a desired frequency. The monochromators needed for the detection of the CARS signals are automatically positioned at the frequency of the generated CARS laser beam. The first experiments show the rovibrational transitions of H_2 as expected. The introduction of a refence branch (currently under construction) in the set-up will further decrease the detection limit (current detection limit ~ 10^{19} m^{-3}).

Contents

1 Introduction

In the group Equilibrium and Transport in Plasmas of the Physics Department of the Eindhoven University of Technology two kinds of plasma are under study; the Induction Coupled Plasma (ICP) and the cascaded arc plasma.
ICP plasmas can be used for the analysis of elements in gaseous environments. Some examples are the monitoring of exhaust gases in waste disposal plants[1] and illumination (QL lamps). Cascaded arc plasmas can serve as a stable light source for spectroscopic techniques[2] or as deposition source of amorphous silicon or carbon for use in solar cells or coatings. Another possible use is as a ion source for positive or negative hydrogen ions or hydrogen atoms.
The carrier gas in these cascaded arc plasmas is argon since this is an inert noble gas. A cascaded arc plasma of pure argon was investigated by Van de Sanden[3]. For etching or deposition purposes reactive components can be added e.g. hydrogen, carbon or silicon. These admixtures change the physical properties of the plasma elements[4,5,6]. The aim of the fundamental research is to acquire more insight in the plasmaphysical atomic processes between the particles: atoms, electrons, ions and molecules.
There are several means of characterizing cascaded arc plasmas. One of these is optical emission spectroscopy[3] (OES), which provides information about the densities of excited atoms in the plasma. Other diagnostics are e.g. Fabry-Pérot interferometry[7] (to measure electron density and heavy particle temperature from broadening and shifting of spectral lines), laser induced fluorescence[8] (LIF)(densities of excited levels by total deexcitation), Thomson-Rayleigh scattering[3] (which provides information about the densities and temperatures of electrons and neutral particles) and Coherent Anti-Stokes Raman Scattering[9] (CARS) (for measuring the densities of rovibrationally excited molecules).

This report is divided in two sections:
In the first part optical emission spectroscopy is used to determine the population of excited levels in the hydrogen atoms in the plasma, thus providing insight in the hydrogen kinetics in the region in front of the stationary shock. This shock is a result of the transition from a supersonic expansion near the nozzle to a subsonic expansion further in the vessel[3]. This part of the report consists of 5 chapters. Chapter 2 gives a general theoretical survey of the plasma under study. The principle behind OES is briefly discussed in chapter 3. In chapter 4 the experimental conditions and set-up are discussed. The results of the experiments are presented and discussed in chapter 5 and in chapter 6 conclusions are drawn and summarized.
The second part describes the initial stages of the CARS experiments. This report gives a brief introduction into Coherent anti-Stokes Raman Scattering theory in Chapter 7. In chapter 8 some initial tests of the diagnostic are mentioned as well as the first results of CARS measurements. A pascal program was written in order to be able to perform computer controlled measurements. The manual to this program can be found in appendix B.

2 Theory

2.1 Electronic transitions

If an electron in an atom or molecule makes a transition from a higher excited state p to a lower state q it loses energy $E_{pq} = E(p) - E(q)$ by means of radiation, $E_{pq} = h\nu_{pq}$ (with h Planck's constant and ν_{pq} the frequency of the emitted photon). The intensity of this radiation of frequency ν_{pq} provides information about the occupation of level p, which is a result of several collisional and radiative processes. The main processes are listed below.

1) Radiative processes: absorption and spontaneous emission of radiation between the levels p and q:

$$A(p) \leftrightarrow A(q) + h\nu \tag{2.1}$$

Stimulated emission can be written as:

$$A(p) + h\nu \rightarrow A(q) + h\nu + h\nu$$

2) In collisional processes usually the electrons provide the energy needed for a transition. Collisional excitation and deexcitation can thus be written as:

$$A(p) + e^- \leftrightarrow A(q) + e^- \tag{2.2}$$

and collisional ionisation and the reverse process, three-particle recombination as:

$$A(p) + e^- \leftrightarrow A^+(1) + e^- + e^-$$

The ionisation process will only occur if the electron energy is larger than the ionisation energy or the energy difference between two successive levels (which can easily be the case for higly excited states).

The plasma is mainly recombining. The main region where ionisation processes play a substantial role will be inside the arc. In the vessel the deexcitation mechanisms are of more importance than the exciting mechanisms which can be derived from the fact that the b_p-factor (equation (2.10))is smaller than one[10] in the plasma under study[11] (if an extra input of excited levels is present, due to molecular processes, b_p can be larger than one, even for a recombining system). The higher excited states will be mainly populated by three-particle recombination, the lower states by radiative and collisional decay.

In an expanding hydrogen-argon plasma recombination, collisional and radiative transitions are given by:

$$\begin{aligned} Ar^+ + e^- + e^- &\rightarrow Ar^* + e^- \\ H^+ + e^- + e^- &\rightarrow H^* + e^- \end{aligned} \tag{2.3}$$

$$\begin{aligned} Ar(p) + e^- &\leftrightarrow Ar(q) + e^- \\ H(p) + e^- &\leftrightarrow H(q) + e^- \end{aligned} \tag{2.4}$$

and

$$\begin{aligned} Ar(p) &\rightarrow Ar(q) + h\nu_{pq} \\ H(p) &\rightarrow H(q) + h\nu_{pq} \end{aligned} \tag{2.5}$$

In addition to these processes there is also dissociative recombination of ArH^+ ions after associative charge exchange of argon ions and hydrogen molecules:

$$Ar^+ + H_2 \rightarrow ArH^+ + H \tag{2.6}$$

$$ArH^+ + e^- \rightarrow Ar + H^* \tag{2.7}$$

2.2 Densities of excited states

Plasmas are generally not in thermodynamic equilibrium (TE). There are gradients in densities and temperature and energy flows into and out of the plasma. A useful way to describe a plasma which is not in TE is to assume a local thermal equilibrium (LTE) with a certain temperature for electrons and atoms depending on the position in the plasma. For a plasma in LTE the population of an excited level can be calculated from the Boltzmann and Saha equations.

The Boltzmann equation calculates the population of an excited level, n_p, from the density of the ground-state, n_1:

$$\frac{n_p}{g_p} = \frac{n_1}{g_1} \exp\left(-\frac{E_{p1}}{kT_e}\right) \tag{2.8}$$

In this equation k is Boltzmann's constant, T_e the electron temperature, g_p and g_1 are the statistical weights of level p and the ground-state respectively and $E_{p1} = E(p) - E(1)$ the energy difference between the levels.

The Saha equation describes the equilibrium population of an excited level p in terms of the density of the ion-ground-state and the electron-density:

$$\frac{n_p^{Saha}}{g_p} = \frac{n_e n_i}{g_e g_i} \left(\frac{h^2}{2\pi m_e kT_e}\right)^{\frac{3}{2}} \exp\left(\frac{E_{ip}}{kT_e}\right) \tag{2.9}$$

In this equation m_e is the electron mass, n_e the electron density and g_e the spin degeneracy of the electron ($g_e = 2$, the statistical weight for the ion-ground-state is $g_i \approx 5.6$ for argon[12] (under our experimental conditions) and $g_i = 1$ for hydrogen).

Since higher excited states, which lie close to the ionisation level, are mainly populated by three-particle recombination from the ion-ground-state the Saha equation is the more important one for these levels[10]. Therefore $n_p = n_p^{Saha}$ for p large enough.

The plasma under laboratory conditions, however, is usually not in LTE. This means that the Boltzmann and Saha equations are no longer valid. The deviation from the densities predicted by Saha is expressed in the b_p-factor:

$$b_p = \frac{n_p}{n_p^{Saha}} \tag{2.10}$$

If $b_p > 1$ or $b_p < 1$ there is overpopulation or underpopulation, respectively, of level p compared to Saha.

In recombining plasmas three particle recombination is a main source of highly excited atoms. For these levels, close to the ionisation level, b_p approaches 1, meaning these levels are in partial local Saha equilibrium (pLSE)[10].

The Saha equation requires knowledge of the ion density n_i. For pure argon plasmas the ion density is equal to the electron density. In the case of an argon-hydrogen plasma the concentration ratio between argon and hydrogen ions can be calculated if the following assumption is made: Two levels which are to be compared have the same b_p factor. Therefore it is necessary to compare two highly excited states which are in Saha equilibrium with their continuum. Further the difference in ionisation energy of the two levels should be small for the temperature dependence in the Saha equation to be of little influence. The ion concentration ratio is then given by the ratio of the two respective Saha equations[11]:

$$\frac{[Ar^+]}{[H^+]} = \frac{(n_p / g_p)^{Ar}}{(n_p / g_p)^{H}} \frac{g_i^{Ar}}{g_i^{H}} \exp\left(-\frac{E_i^{Ar} - E_i^{H}}{kT_e} \right) \tag{2.11}$$

A possibility to calculate the population of a certain level stems from the transport (preservation of mass) formula:

$$\frac{\partial n_p}{\partial t} + \nabla \cdot \{n_p w_p\} = \left(\frac{\partial n_p}{\partial t} \right)_{CR} \tag{2.12}$$

In this equation the first term on the left hand side denotes the time dependence of the population of level p for an observer moving at the same speed as the particles, the second term is due to the movement (at drift velocity w_p) of the particles. The term at the right side contains the gain and loss of particles at level p due to collisional-radiative processes. Since the transition probabilities of hydrogen are large this term will be of much more importance than the drift term on the left. Therefore the drift term can be neglected in our case.

Equation (2.12) can further be simplified by using the quasi steady state solution (QSSS)[13], which is based on the following assumptions: Deexcitation and excitation to or from the ground state and ionisation and recombination to or from the ion state are fast enough to be able to describe n_p by the densities of ground and ion state and the temperature at any moment. Only excited states are considered, and not the ground state or ion state (which contain the main part of the particles).

In the QSSS approximation the only remaining terms are the gain and loss due to collisional-radiative processes:

$$0 = \left(\frac{\partial n_p}{\partial t} \right)_{CR} = Gain + Loss \tag{2.13}$$

With the processes mentioned in the previous paragraph equation (2.13) can be written as[13]:

$$\begin{aligned} & n_e \sum_{j \neq p} n_j K_{jp} - n_e n_p \sum_{j \neq p} K_{pj} + \sum_{j>p} n_j \Lambda_{jp} A_{jp} \\ & - n_p \sum_{j<p} \Lambda_{pj} A_{pj} - n_e n_p K_{pi} + n_e^2 n_i K_{3PR} + n_i n_{mol} K_{diss.rec.} = 0 \end{aligned} \tag{2.14}$$

In this equation the seven terms on the left are excitation, deexcitation, cascade radiation, spontaneous emission, ionisation, three particle recombination and dissociative recombination respectively. The K_{jp} factors denote the rate constants for the collisional (de)excitation from j to p, A denotes the transition probability, Λ the escape factor for radiation, $0<\Lambda<1$ ($\Lambda=1$ for radiation of transitions not to the ground state), which accounts for reabsorption of radiation by the plasma and n_e, n_i, n_j ,n_p and n_{mol} the densities of electrons, ions, level j and p and molecules respectively. The rate constants K can be calculated from the velocity of the particles, which is assumed Maxwellian, and the cross-section, calculated using a hard spheres approximation.

In our plasma one of the main sources of excited level population is three particle recombination. This process will populate highly excited states which will in turn populate lower levels by cascaded collisional deexcitation and (for low levels) spontaneous emission. Therefore the number of atoms entering a certain level can be approximated by the number of recombined ions (this is even exactly true for cascaded deexcitation which never bypasses this level). For high levels, however, collisional excitation will also play a substantial role in the population of the levels, making actual calculation of populations more difficult. In the

low level region the rate constants for excitation are small due to large energy differences between the levels, leaving only collisional and radiative deexcitation as possibilities of loss of excited atoms. This allows for a simple balance to be made: The input of a level, approximated by three particle recombination, must be equal to the output of that level by collisional and radiative deexcitation. It can be shown that for the levels calculated later in this paper, level 2 and 3 of hydrogen, radiative deexcitation is the dominant process. This simplifies equation (2.14) to:

$$n_e^2 n_i K_{3PR} = n_p \sum_{p>j} \Lambda_{pj} A_{pj} \tag{2.15}$$

3 Line intensities

Absolute line-intensities can provide information about the absolute population of excited levels. To be able to use the measurements for this purpose some assumptions are to be made:

1. The argon ions are singly ionised. This means that for low hydrogen concentrations the Argon ion density n_i can be taken equal to the electron density n_e.
2. The plasma is cylindrically symmetric, thus allowing for a tomographic Abel-inversion to be used.
3. The plasma is optically thin for all measured lines (except for 4p $\rightarrow$ 4s and 4s $\rightarrow$ 3p transitions in argon and the 2 $\rightarrow$ 1 transition in hydrogen), which means that $\Lambda = 1$.
4. The light emission of the plasma is isotropic.

The light emitted due to an electronic transition from a higher level p to a lower level q is proportional to the population $n(p)$ of level p, the transition probability A_{pq} and photon energy $h\nu_{pq}$ [14].

$$P_{pq} = \frac{h\nu_{pq}}{4\pi} A_{pq} n_p \tag{3.1}$$

with the radiated power P_{pq} in $Jsr^{-1}s^{-1}m^{-3}$.

Since the measurements yield lateral scans of the intensity of the radiation emitted by the plasma (in photon-counts) a tomographic Abel-inversion technique[14] is necessary for obtaining a radial profile of the density of a certain level.
Before the actual Abel-inversion a calibration is necessary. The lateral profile of photon-counts is compared with the intensity of a tungsten ribbon lamp, since for this light source the intensity as a function of temperature and wavelength is well known. The ribbon lamp, however, is a radiating surface as opposed to the radiating volume of the plasma.
It can be shown[14] that for spectral lines with widths smaller than the apparatus profile $\Delta\lambda$ (= 0.16 nm) the ratio of the intensities of a line, I_p , and the ribbon lamp, I_b, obeys the following equation[13]:

$$\frac{I_p}{I_b} = \frac{s \cdot h\nu_{pq}}{4\pi} \frac{A_{pq}}{\Delta\lambda \cdot B(\lambda,T)} n_p \tag{3.2}$$

with s the thickness of the scanned layer in the plasma and $B(\lambda,T)$ the intensity of the tungsten ribbon lamp. This means that the population of a certain level p can be calculated from the ratio of the mentioned intensities:

$$n_p = \frac{4\pi \cdot \Delta\lambda}{A_{pq}} \frac{I_p}{I_b} \frac{B(\lambda,T)}{s \cdot h\nu} \tag{3.3}$$

In this equation the plasma emission depends on the lateral position; $I_p = I_p(x)$. The ribbon lamp emission depends on the radial position; $I_b = I_b(r)$. Abel inversion of I_p however will change its dependence into radial dependence.
The use of a photomultiplier tube (PMT) to detect the emitted light means that not the intensity of a line is measured, but a number of photons, which, if the response of the PMT is linear, will be proportional to the intensity of the line.
With N_p, the number of pulse-counts in the Abel-inverted profile of a certain line, and N_b, the number of counts of the ribbon lamp calibration, equation (3.3) can be written as:

$$n_p = \frac{4\pi \cdot \Delta\lambda}{A_{pq}} \frac{N_{deVos}}{N_b} N_p \tag{3.4}$$

In this equation $N_{de\ Vos}$ is the number of photons emitted by the ribbon lamp, corrected for the 92 % transmission of the window of the lamp; $N_{de\ Vos} = 0.92\ B(\lambda,T)/h\nu$.

In equation (3.4) $\Delta\lambda$ is the only parameter depending on the optical path from the plasma to the PMT. This means that the calibration with the ribbon lamp must be performed under the same conditions as the actual measurement so that any transmission coefficients will be accounted for.

4 The experimental set-up

4.1 The cascaded arc

The hydrogen and argon lines are measured in an expanding plasma jet. The plasma is created in a cascaded arc and expands supersonically into a vessel. This vessel is pumped by a pumping system to maintain a pressure of 0.3 torr. Figure 4.1 shows a drawing of the cascaded arc. The arc as a whole can be moved inside the vessel in the axial direction (z-direction), thus allowing for measurements at different axial positions with fixed optical equipment.
In order to be able to study the effects of injecting hydrogen directly into the beam, where it ionises and deexcites, or into the vessel, where it can only be excited by other mechanisms, the set-up has two points for injecting hydrogen. The first option is to admix the hydrogen to the argon gas which flows into the cathode area, the second is to let the hydrogen gas enter the vessel in front of the cathode so it can spread throughout the vessel.

4.2 The line-intensity diagnostic

The light emitted by the plasma is partially transmitted through one of the windows of the vessel. At this window the line-intensity diagnostics start with a mirror and a pair of lenses focussing the detection volume at a pinhole (∅ 0.5 mm) (see figure 4.2). Another pair of lenses focusses the pinhole at the entrance slit of the Bentham M300 monochromator (1200 groove/mm grating). A GG495 low-pass filter is placed in front of the monochromator with wavelengths over 500 nm. Then the intensity of a certain line in the spectrum of hydrogen or argon is measured with a Hamamatsu R1617 photomultiplier tube (PMT). This signal is sent through a LRS model 612 amplifier, LRS model 623 octal discriminator and a LRS model 688AL level adapter before being transferred to a PC for storage and processing.
The size of the detection-volume is limited by the image of the pinhole and entrance slit of the monochromator at the plasma. Since the first pair of lenses enlarges the pinhole by a factor of 3/2 the detection volume is at least 0.75 mm high. The image of the entrance slit at the detection volume is 120 μm being the width of the detection volume. The solid angle, $5 \cdot 10^{-3}$ sr, is determined by the diameter of the first lens. For making lateral scans of the plasma the second mirror can be turned with a stepping motor, resulting in steps of minimal 26 μm in the plasma.
The monochromator has a resolution of 2.7 nm/mm and an entrance and exit slit of 60 μm, thus yielding a wavelength-resolution of 0.16 nm. Earlier experiments[14] show that this is enough to resolve the measured lines.
For calibration purposes our experimental set-up used two tungsten ribbon lamps. The first was placed inside the vessel to calibrate the optical path from plasma to PMT and to make lateral calibration scans. The second was placed outside the vessel and, with an extra lens slid into the optical path, could be used to calibrate the path from the rotating mirror to the PMT, at only one lateral position. This calibration could be performed without going through the laborious phase of opening the vessel at the risk of contamination by dust or hydrogen from water in the air. This second ribbon lamp made it possible to perform a secondary calibration between the measurements, thus allowing for better control of the alignment of the set-up.

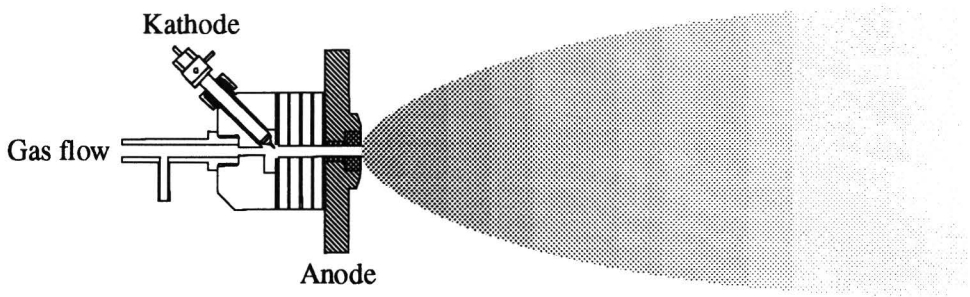

Figure 4.1: The expanding cascaded arc. On the left the arc and on the right the expanding plasma.

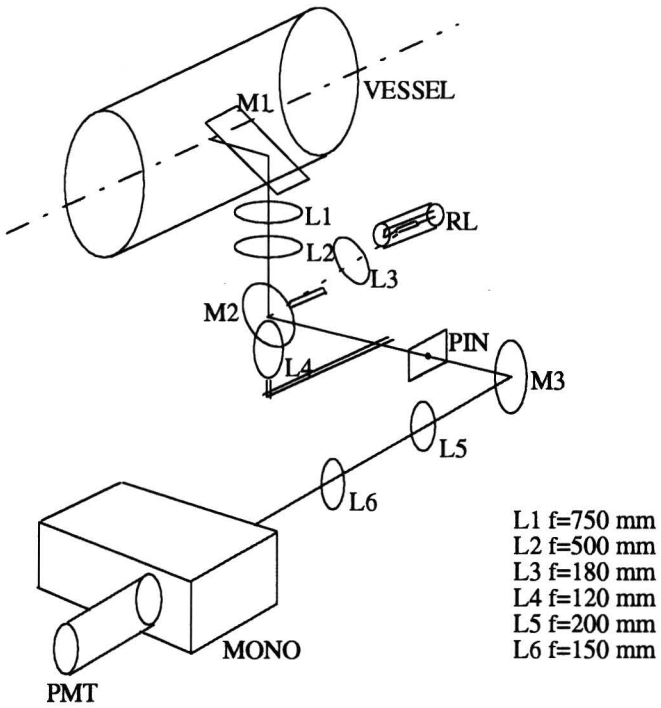

Figure 4.2: A schematic of the line-intensity set-up, with L1..L6 denoting lenses (L4 can be slid into the optical path on a rail), M1..M3 mirrors (M2 can rotate to make lateral scans of the plasma),RL a tungsten ribbon lamp, PIN the pinhole, MONO the monochromator and PMT the photomultiplier tube.

5 Experiments, results and discussion

5.1 Experiments

The experiments consist of sets of lateral scans of the intensities of hydrogen Balmer lines and argon lines at several (volume) percentages of (molecular) hydrogen injected either directly into the arc or into the vessel. The axial position for the measurements was maintained at 20 mm from the nozzle. Each scan consists of photon-counts at 81 positions in the plasma 1.25 mm apart. These counts were calibrated with the lateral scan of pulse-counts of the tungsten ribbon lamp and Abel-inverted to give a radial profile of the population of the level.

The plasma conditions were held constant for all measurements. The total gas flow through the arc was 3500 ml/min during hydrogen injection in the arc. For measurements with hydrogen injected in the vessel the total gas flow (argon in the arc plus hydrogen in the vessel) was also kept at 3500 ml/min. The pumping system maintained a pressure inside the vessel of 0.3 Torr. The current through the arc was set at 45 A, this means a voltage from 105 V for a pure argon plasma up to 140 V for 20 percent of hydrogen injected into the arc.

5.2 Results and discussion

Figure 5.1 shows the population (divided by the statistical weight) of a number of excited hydrogen levels. The first remark to be made is that the percentages of hydrogen injected into the arc are not necessarily comparable with the percentages of hydrogen injected into the vessel. This is a result of the fact that the time that the hydrogen atoms or molecules remain in the vessel may differ for both situations. If the time that the hydrogen stays in the vessel is larger than the time needed for recirculation inside the vessel, however, the difference in residence time is of little importance. The information obtained from these n_p/g_p measurements will be discussed in the next paragraphs.

5.2.1 Introduction

The most obvious difference between the n_p/g_p plots for hydrogen injection into the arc and the vessel is that injection in the arc produces more excited states (up to level 14 or 15 can be measured) than injection in the vessel (up to level 6). This is related to the mechanisms responsible for the excitation of atomic hydrogen.
For hydrogen injection in the arc there are two different mechanisms. The first is three particle recombination (equation (2.3)). This requires ionised hydrogen, which can be produced inside the arc. This process populates high levels. The second is dissociative recombination (equations (2.6) and (2.7)), which requires molecular and atomic hydrogen and ionised argon from the arc, and populates lower levels. This mechanism can also be present when injecting hydrogen into the vessel. Another big difference between injection in the arc and the vessel is the dependence of the population of excited levels on the concentration of hydrogen injected. This phenomenon is discussed in more detail in the following two paragraphs.

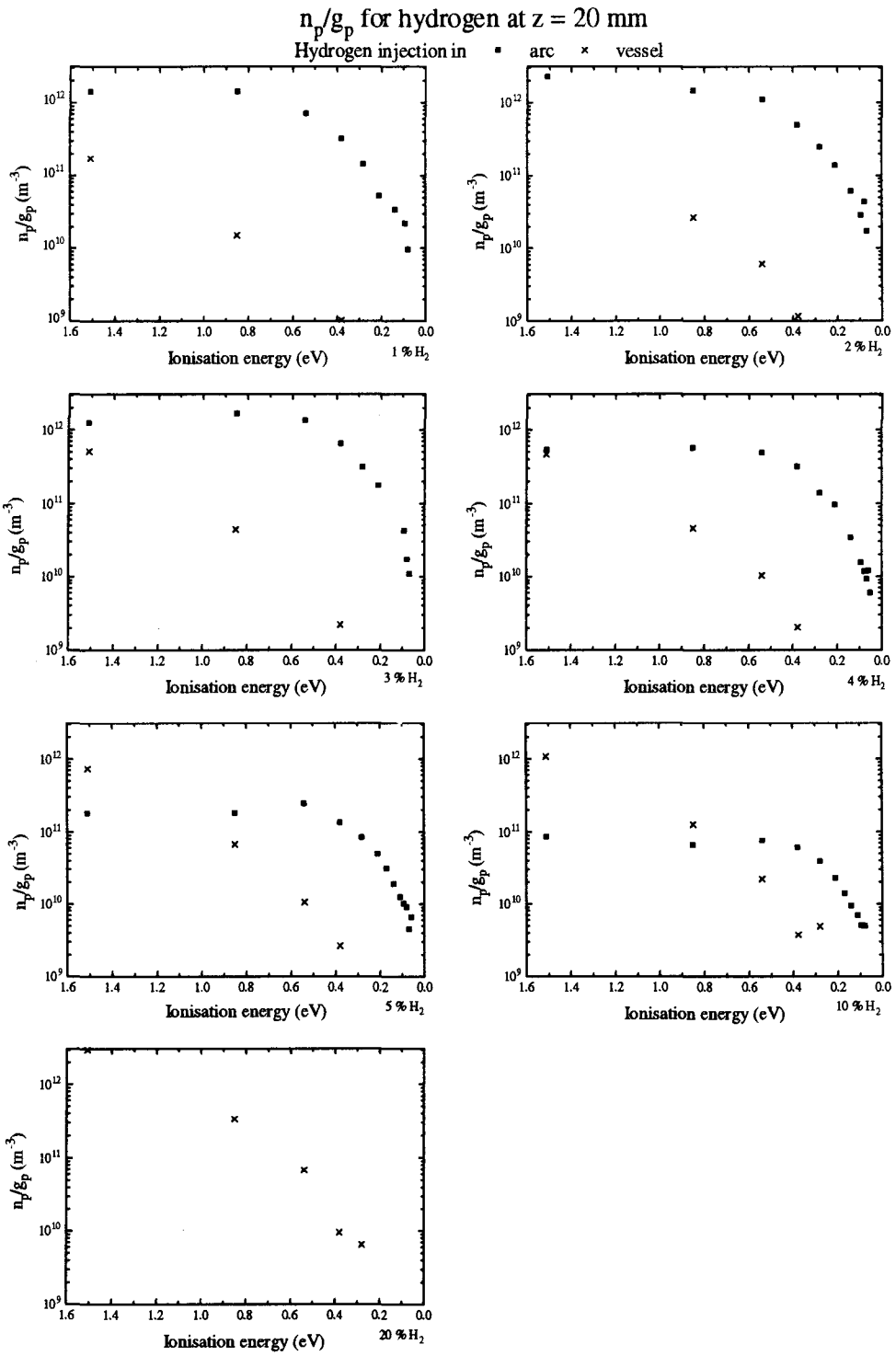

Figure 5.1: n_p/g_p as a function of ionisation energy of hydrogen levels, for 1 to 20 percent hydrogen and injection in arc or vessel. note that for injection in the vessel only the lower states are excited whereas injection in the arc also excites the higher levels.

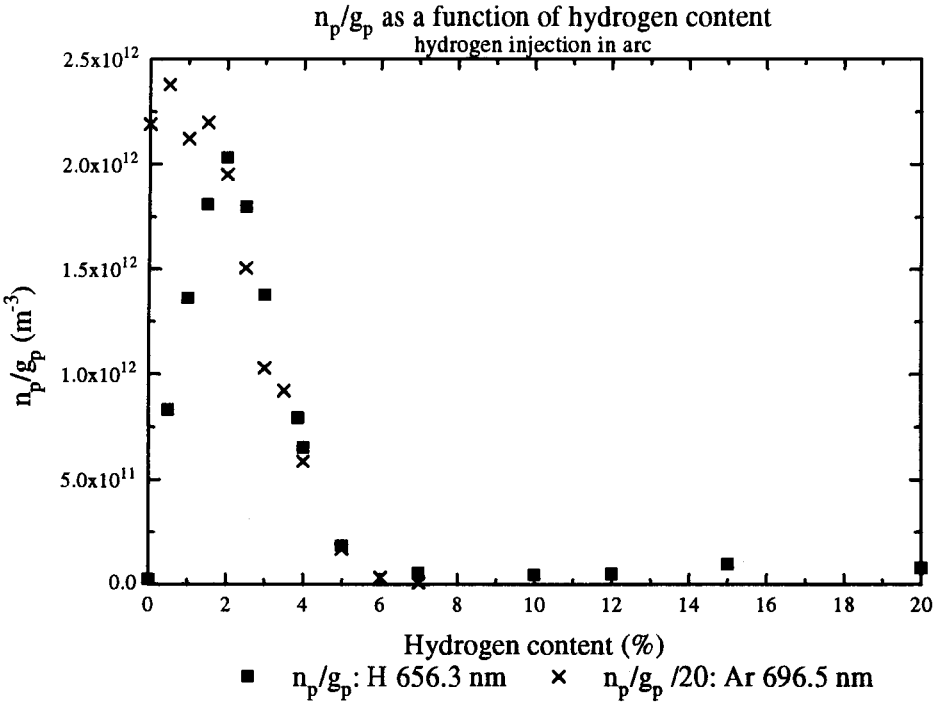

Figure 5.2: n_p/g_p for H_α (656.3 nm) and the argon 696.5 nm line, as a function of hydrogen content for injection in the arc.

5.2.2 Hydrogen injection in the arc

The intensity of the H_α line (transition from the hydrogen p=3 to the p=2 level), for hydrogen injection in the arc, is displayed in figure 5.2. The population of the third level rises until the hydrogen content of the gas mixture is about 2 percent, this rise is mainly due to the fact that there is more hydrogen present for three particle recombination whereas the Ar^* emission (and therefore the electron density) remains nearly constant. At two percent the population of the third level reaches a maximum. The partial population by three particle recombination can be calculated from equation (2.15), which in this case has the form:

$$\frac{1}{3} n_e^2 n_{H^+} K_{3PR} = n_3 A_{3\to 2} + n_3 A_{3\to 1} \qquad (5.1)$$

The factor 1/3 is a result of the fact that hydrogen atoms in the fourth excited state have three levels to deexcite to, with approximately the same probabiltities, only one of which is measured (namely the third level).The hydrogen ion density can be calculated from the argon ion density and the ion concentration ratio (icr=75), $n_{H^+} = n_{Ar^+} / icr \approx n_e / icr$. For 2 % hydrogen injection the electron density is n_e = $3.2 \cdot 10^{19}$ m^{-3} (from Thomson-Rayleigh measurements by Beurskens[15]) and the rate constant for three particle recombination, K_{3PR} = $1.7 \cdot 10^{-35}$ $m^6 s^{-1}$ [16]. The transition probabilities are $A_{3\to 2}$ = $4.41 \cdot 10^7$ s^{-1} and $A_{3\to 1}$ = $5.575 \cdot 10^7$ s^{-1}. With these values the population of the third level can be calculated to be n_3/g_3 = $1.4 \cdot 10^{12}$ m^{-3}. This agrees with the experimental value of n_3/g_3 = $2.3 \cdot 10^{12}$ m^{-3}, implying that three particle recombination is the dominant process at this position in the plasma (20 mm from the nozzle at the plasma axis). From 2 to 5 percent the intensity of H_α decreases rapidly. This effect is due to the fact that the efficiency of the arc deteriorates for higher hydrogen contents,

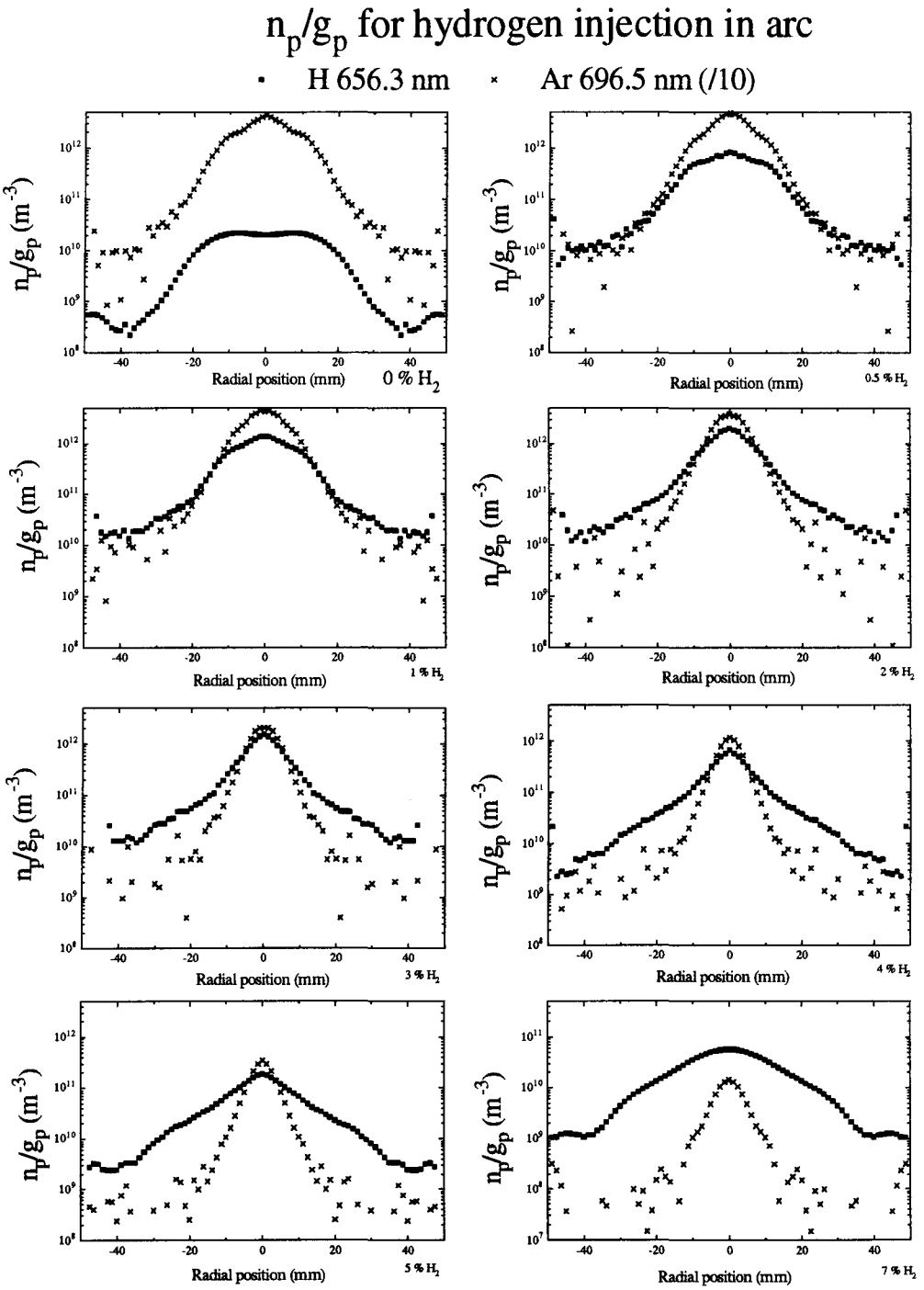

Figure 5.3: Comparison of the line-intensity profiles of hydrogen and argon lines as a function of the amount of hydrogen injected in the arc. The argon profile intensities are devided by 10 for clarity of the figures.

causing the electron density to drop (similar to the drop in the argon line's intensity) and to the fact that increasing the amount of hydrogen in the gas mixture will change the ion concentration ratio. Because of its lower ionisation energy hydrogen is ionised more easily than argon. Therefore the ratio of hydrogen ions to argon ions increases faster than the ratio of the respective atoms. In the last part of the plot, from 5 to 20 percent of hydrogen, the

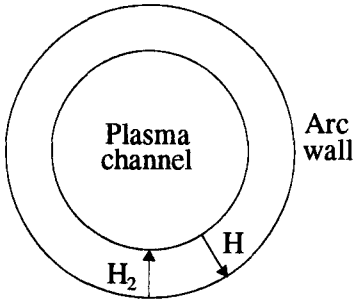

Figure 5.4: Formation of a sheath of molecular and atomic hydrogen around the plasma channel inside the arc. This sheath narrows the effective channel for the plasma.

population of the hydrogen level remains stable, implying there is an effect that, although there are hardly any argon ions left in the arc, populates the hydrogen levels. This process will either be three particle recombination of hydrogen ions or dissociative recombination after associative charge exchange of hydrogen molecules with, in this case, hydrogen ions, since argon ions are no longer available in the plasma. The partial population of the third level by three particle recombination can again be calculated. With an estimated value of $n_e \approx 5 \cdot 10^{17}$ m^{-3} it follows that this partial population is equal to $n_3/g_3 = 2.4 \cdot 10^9$ m^{-3} whereas the experimental value is $n_3/g_3 = 5 \cdot 10^{10}$ m^{-3}, indicating that three particle recombination is not the only mechanism populating the excited hydrogen states. Figure 5.3 shows radial profiles for hydrogen and argon lines. The excited argon line appears to get narrower as the hydrogen content increases, implying that the argon ion profile will get narrower too. This could be a result of dissociative recombination with molecular hydrogen, which enters the plasma beam from the outside, which indicates a recirculation flow of hydrogen outside the plasma, near the vessel wall[10,15]. The fact that this narrowing of the argon profile is not found when injecting hydrogen directly into the vessel (next paragraph), however, indicates that the recirculation flow near the vessel wall has not yet entered the plasma beam at 20 mm from the nozzle. Another possible cause of the of the narrowing of the radial argon line profile is the formation of a H_2 sheath around the plasma inside the arc[15] due to diffusion of H and H_2 (see figure 5.4). This sheath narrows the plasma channel (and profile) and can cause additional dissociative recombination on the plasma edge, in the expansion, with the hydrogen molecules that surrounded the plasma channel inside the arc.

In the case of hydrogen injection in the arc the b_p for H_α (E_i = 1.51 eV) decreases if the hydrogen concentration rises, see figure 5.5, indicating a growing deviation from the Saha equilibrium. The b_p plots for hydrogen in the arc also display a maximum which lies around level 6 or 7 for 1 percent of hydrogen and shifts to higher levels if the hydrogen content increases. This maximum has been reported before[6,14] and was explained as a result of specific excitatation of those levels. This means that there must be other processes, besides the main process, three particle recombination, which produce some excited hydrogen atoms since excitation by only three particle recombination would result in a monotone b_p plot (no maximum near level 7). The fact that the b_p curves become flatter when the hydrogen content increases indicates that these other processes loose significance if the plasma changes from containing mainly argon ions to mainly hydrogen ions. This leads to the conclusion that dissociative recombination might be a second source of excited hydrogen atoms when injecting hydrogen molecules into the arc.

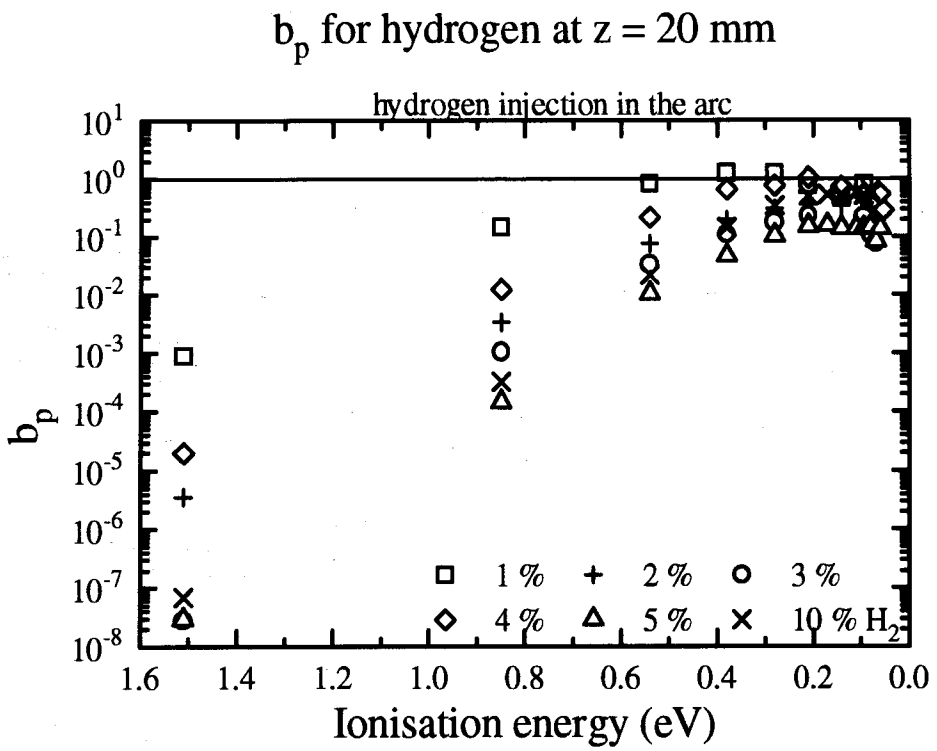

Figure 5.5: Deviation from Saha, b_p, for hydrogen injection in the arc. Note that for an increasing hydrogen content the deviation increases, this means that n_e and T_e decrease when the hydrogen content rises.

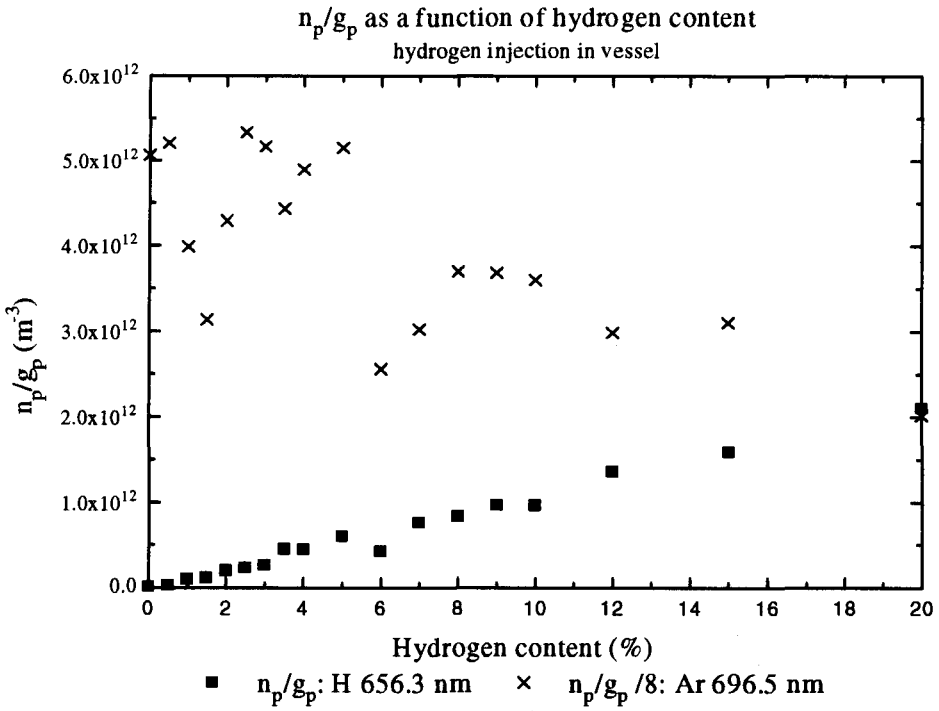

Figure 5.6: n_p/g_p for H_α (656.3 nm) and the argon 696.5 nm line as a function of hydrogen content for injection in the vessel.

5.2.3 Hydrogen injection in the vessel

In figure 5.6 it can be seen that for hydrogen injection in the vessel the population of the third excited level of hydrogen increases with increasing hydrogen concentration up to 20 percent. The argon density appears to slowly decrease as a result of the increasing rate at which dissociative recombination can occur, since the amount of molecular hydrogen increases. A small part of the decrease in argon density is due to the fact that the total argon flow through the arc diminishes since the total gas flow into the vessel is maintained at 3.5 slm. Figure 5.7 shows the population profiles for injection in the vessel. The hydrogen profiles display a form with a maximum on each side of the center. This is a result of the fact that hydrogen is now injected in the vessel and has to diffuse into the expanding jet of the argon plasma. The intensity of the hydrogen profiles rises with increasing hydrogen content and the maxima shift towards the center, both as a result of the increased density of molecular hydrogen. Since three particle recombination of hydrogen in the arc is now impossible, dissociative recombination is left as a means of creating excited hydrogen levels. Figure 5.1 showed that, in the case of injection in the vessel, no highly excited states could be measured but only the levels 3 to 6. In the case of hydrogen injection in the vessel dissociative recombination can produce excited hydrogen atoms by the following process:

$$\begin{aligned} Ar^+ + H_2 &\rightarrow ArH^+ + H \\ ArH^+ + e^- &\rightarrow Ar + H(p=2) \end{aligned} \qquad (5.2)$$

This process mainly produces excited hydrogen atoms at level 2 since the maximum available energy for the excitation of hydrogen atoms is smaller than the energy needed to excite level three. From level 2 transitions can be made to the ground state and to higher levels:

$$\begin{aligned} H(p=2) &\rightarrow H(p=1) + h\nu \\ H(p=2) + e^- &\rightarrow H(p=3) + e^- \end{aligned} \qquad (5.3)$$

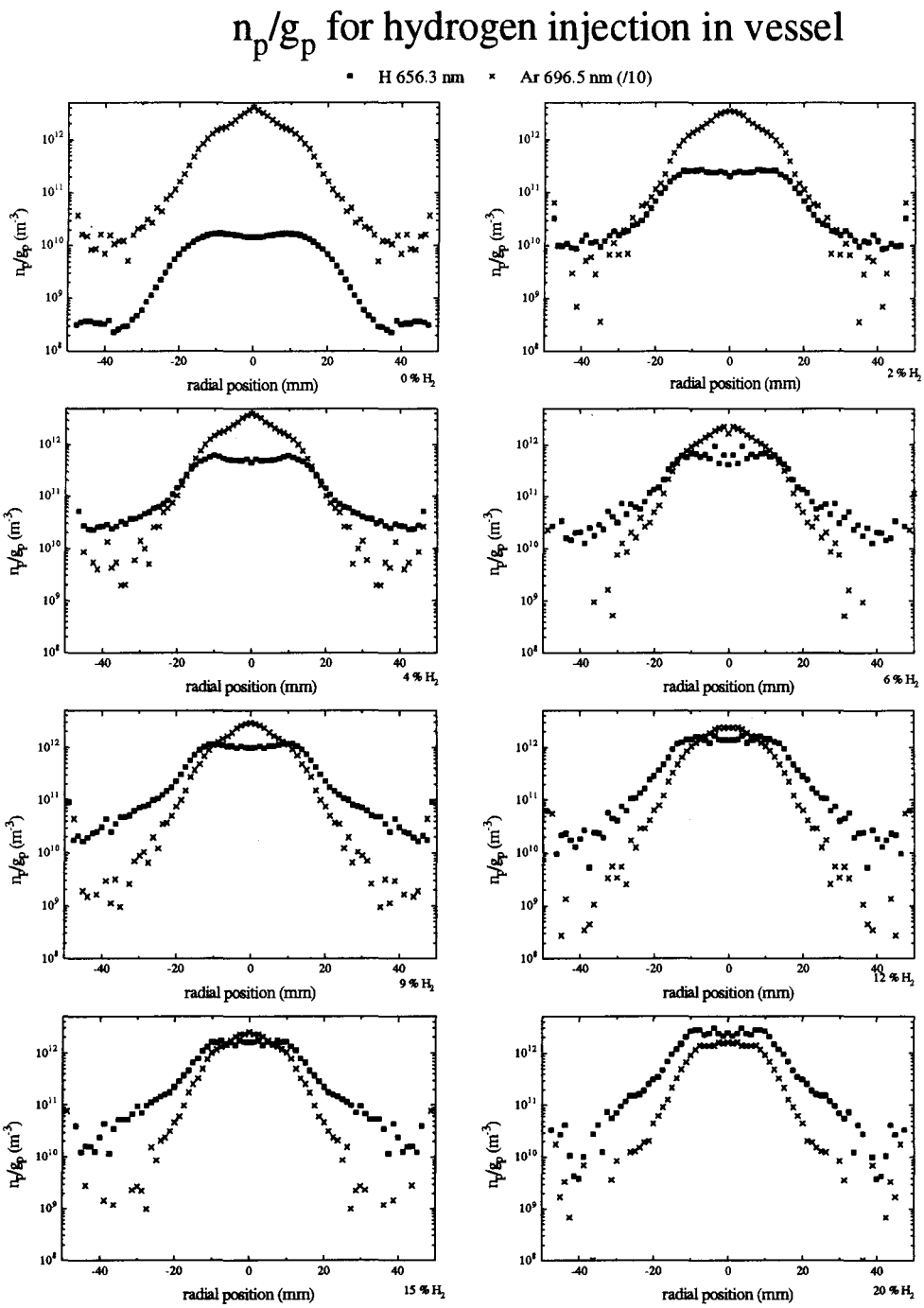

Figure 5.7: Comparison of the intensity of hydrogen and argon lines as a function of the amount of hydrogen injected into the vessel. The intensity of the argon line is devided by 10 for clarity of the figures.

Therefore the populations of the excited levels of atomic hydrogen mainly depend on the density of molecular hydrogen. This means that if the density of molecular hydrogen was known the density for the excited hydrogen atoms could be calculated, or vice versa, from the

QSSS of the particle balance in which the argon ion density is approximated by the electron density:

$$n_e n_{H_2} K_{diss.rec} - n_{H(n=2)} A_{2\to 1} = 0 \tag{5.4}$$

$$n_e n_{H(p=2)} K_{2\to 3} - n_{H(p=3)} A_{3\to 2} - n_{H(p=3)} A_{3\to 1} = 0 \tag{5.5}$$

with the rate constant of dissociative recombination $K_{diss.rec}$ = $1.1 \cdot 10^{-15}$ $m^3 s^{-1}$ [17](for T = 2000 K), the transition probability from level two to one, $A_{2\to 1}$ = $4.699 \cdot 10^8$ s^{-1}, $K_{2\to 3}$ = $1.23 \cdot 10^{-18}$ $m^3 s^{-1}$ (from a hard sphere approximation of the collisional cross section), $A_{3\to 1}$ = $5.575 \cdot 10^7$ s^{-1} and $A_{3\to 2}$ = $4.41 \cdot 10^7$ s^{-1}. From the electron density, n_e = $3 \cdot 10^{19}$ m^{-3} and the density of the third excited atomic level $n_{H(p=3)}/g_3$ = $1.7 \cdot 10^{11}$ m^{-3} we can calculate the population of the second level to be $n_{H(p=2)}/g_2$ = $1.0 \cdot 10^{18}$ m^{-3} and n_{H_2} = $1.1 \cdot 10^{23}$ m^{-3}. Thomson-Rayleigh measurements performed by Beurskens[15] yield a neutral density of n_0 = $9.3 \cdot 10^{20}$ m^{-3} at z = 20 mm, which is less than the calculated molecular hydrogen concentration. This discrepancy implies that the excitation of the levels three and up can not be a result of dissociative recombination of argon ions with molecular hydrogen populating the p=2 level and excitation from level 2 to higher levels. This means there has to be a process which excites level three directly. A possibility is dissociative recombination of argon ions with rovibrationally excited hydrogen molecules, $H_2^{v,J}$:

$$\begin{aligned} Ar^+ + H_2^{v,J} &\to ArH^{+,v',J'} + H \\ ArH^{+,v',J'} + e^- &\to Ar + H(p=3) \end{aligned} \tag{5.6}$$

The vibrationally excited hydrogen molecules could be a result of association of atomic hydrogen at the steel vessel wall[15,18]. The vibrational energy of the hydrogen molecule (2 eV) can be transferred to ArH^+, thus being added to the internal energy of ArH^+ caused by the exothermity of the charge exchange reaction[19,20]. In this case the internal rovibrational energy of the ArH^+ ion can be enough for the hydrogen atom to be excited to level 3 or 4[21](see figure 5.8). We can assume a distribution of excited atomic hydrogen levels according to Boltzmann with level 3 or 4 as a quasi ground state. The results of this calculation are shown in figure 5.9. This figure indicates that if level 3 and 4 are populated by dissociative recombination, the other levels can be populated by collisional excitation at this temperature (T_e = 0.17 eV ≈ 2000K). The density of vibrationally excited hydrogen molecules, $n_{H_2^{v,J}}$, can now be calculated from:

$$n_e n_{H_2^{v,J}} K_{rec} - n_{H(p=3)} A_{3\to 2} - n_{H(p=3)} A_{3\to 1} = 0 \tag{5.7}$$

With the value of n_e = $3 \cdot 10^{19}$ m^{-3} and $A_{3\to 1}$ = $5.575 \cdot 10^7$ s^{-1} the density of vibrationally excited hydrogen molecules can be calculated to be $n_{H_2^{v,J}}$ = $9.3 \cdot 10^{15}$ m^{-3}. An estimate for the total molecular hydrogen density is in this case one percent of the background gas, $n_{H_2,est.}$ = $1.0 \cdot 10^{19}$ m^{-3} which implies that only a small part of the molecular hydrogen needs to be vibrationally excited in order to obtain the populations of excited atomic levels as measured.

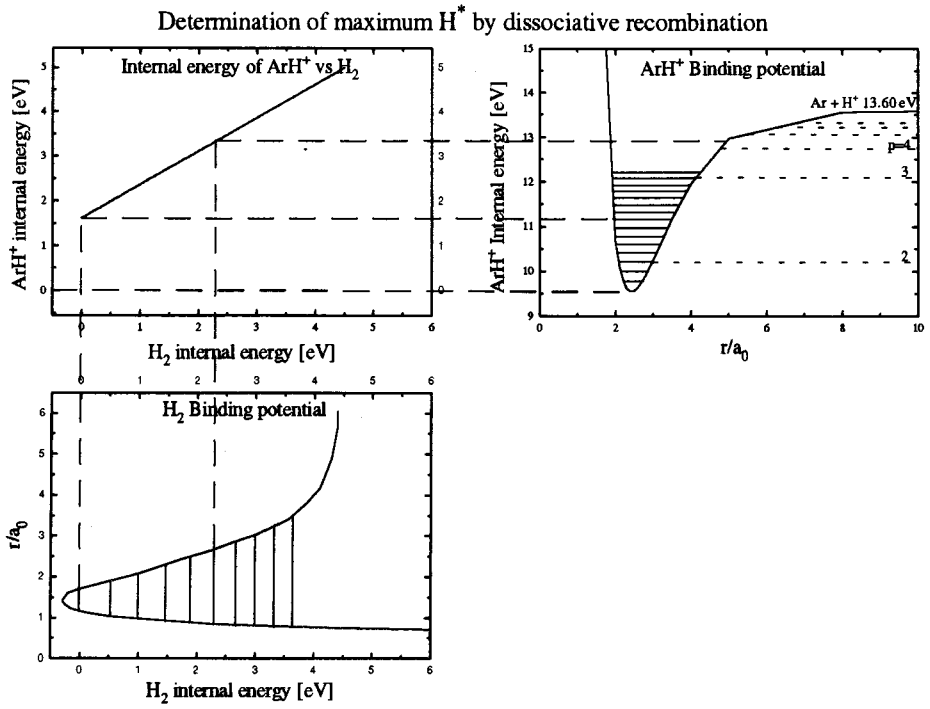

Figure 5.8: Determination of the maximum attainable excited level of atomic hydrogen by dissociative recombination of a rovibrationally excited argon-hydrogen molecular ion. The lower graph on the left represents the potential curve of a hydrogen molecule[22]. With the relation between the rovibrational energy of H_2 and ArH^+ (top left[21]) the corresponding internal energy of the ArH^+ molecular ion[23] (top right) can be determined. The rovibrational energy of ArH^+ determines the highest level of atomic hydrogen (top right, right side) which can be populated.

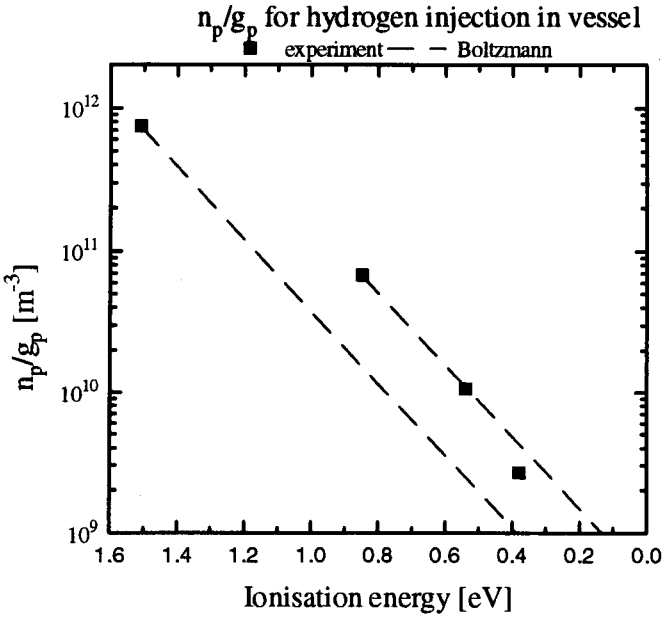

Figure 5.9: n_p/g_p for 5 % hydrogen injection in the vessel as measured. The dashed lines represent the densities calculated from a Boltzmann equilibrium with the third and fourth hydrogen level as quasi ground state (T=2000K). This plot indicates direct population of the p = 3, 4 levels of atomic hydrogen by dissociative recombination of Ar^+ with rovibrationally excited H_2.

6 Conclusions

6.1 Injection in the arc

It has been shown that when injecting H_2 into the arc three particle recombination is the main source of excited hydrogen atoms at 20 mm from the nozzle at the center of the plasma, which is in the region in front of the stationary shock. This can be seen from the fact that relatively high levels (up to p=15) are populated. It is also confirmed by calculating the population by three particle population only.

The intensity of the H_α Balmer line reaches a maximum for 2% of H_2 admixed to the argon gas which flows into the arc. At higher concentrations of H_2 this intensity decreases. This is a result of changes inside the arc since this phenomenon was not observed when injecting hydrogen into the vessel. The efficiency of the arc will decrease when more hydrogen is injected resulting in a lower electron density. The ratio of argon and hydrogen ions changes faster than the rate of the respective atoms, when increasing the hydrogen content, due to the lower ionisation potential of hydrogen. This causes the argon ion density and (through a decrease of dissociative recombination) the H^* density to decrease . Another phenomenon is the formation of a H/H_2 sheath around the plasma inside the arc[15] which results in a narrowed plasma channel and additional dissociative recombination inside and outside the arc on the plasma edge which also decreases the electron and argon ion density.

6.2 Injection in the vessel

Hydrogen injection in the vessel will prevent H^+ from being formed inside the arc. Therefore virtually no three particle recombination can lead to the formation of H^*. The only means of producing excited hydrogen atoms is dissociative recombination. This results in the excitation of only lower states of hydrogen (up to level 7 was observed).

The intensity of H_α is proportional to the concentration of molecular hydrogen injected into the vessel indicating that the changes of the arc mentioned in the previous paragraph, as observed when injecting H_2 into the arc, are of little importance. The density of the excited hydrogen atoms, however, is too high to be explained by dissociative recombination of Ar^+ with non-excited H_2. Theorethical work performed by De Bari[21] showed that the hydrogen molecules in the recirculation current can gain enough energy from the vessel wall to be able to populate the atomic levels p=3,4 directly. This fact, which seems to be confirmed by the measurements, leads to the conclusion that rovibrationally excited molecular hydrogen must play a substantial role in producing excited atomic hydrogen.

6.3 Future experiments

The production of excited hydrogen atoms, when injecting H_2 in the arc, appears to be dominated by three particle recombination at z = 20 mm at the center of the plasma beam. This implies that the recirculation flow of hydrogen molecules near the vessel wall, which will cause dissociative recombination to occur, does not yet enter the plasma jet at this axial position. Future experiments will be performed to get more insight in the axial dependence of the competing H^* producing mechanisms.

More information about the densities of rovibrationally excited hydrogen molecules will be obtained in future experiments using the new CARS diagnostic. It is not certain, however, that these experiments will be able to show population of the fourth or fifth vibrational level of molecular hydrogen. Population of these vibrational levels is necessary to populate the

electronic p= 3,4 levels of H. The population of these vibrational levels, however, can be smaller than the detection limit of the CARS diagnostic (~10^{19} m^{-3} at this moment).

7 Theory

7.1 Rovibrational transitions

In a diatomic molecule the two atoms are held together by an attractive potential energy. The atoms can vibrate about the position of equilibrium and rotate. For a perfect harmonic vibrator, the quantized vibrational energy can be written as:

$$E(v) = (v + 1/2)h\nu \tag{7.1}$$

with v the vibrational quantum number, h Planck's constant and ν the frequency of the vibrating motion. For the rotational energy one can find[24]:

$$E(J) = \frac{J(J+1)\hbar^2}{2I} \tag{7.2}$$

Here J is the rotational quantum number, $\hbar = h/2\pi$ and I the moment of inertia. The spacing of the vibrational levels will be larger than that of the rotational levels. The total rovibrational energy is the sum of the vibrational and rotational energies and can be written as:

$$E(v,J) = C(v,J)(v + 1/2)J(J+1) \tag{7.3}$$

$C(v,J)$ is a constant and can be calculated from the first two equations. Equations (7.1) to (7.3) are true only if the molecule behaves as an harmonic oscillator and ideal rotor. Since the potential holding the atoms together is not perfectly harmonic in real molecules the vibrational energy will also include higher order terms which can be observed as a decreasing spacing of the vibrational levels with increasing vibrational quantum number. The presence of vibrational motion results in a rotation which deviates from an ideal rotor as well; the rotational energy levels will be spaced closer for higher J as well. This effect will be larger for higher vibrational levels due to the anharmonicity of the vibrational motion. This will result in equation (7.3) being changed to the Dunham series expansion[25]:

$$E(v,J) = \sum_{lm} Y_{lm}(v,J)(v + 1/2)^l J^m (J+1)^m \tag{7.4}$$

Values for coefficients Y_{lm} for various molecules can be found elsewhere[25].

Transitions between rotational and vibrational levels in diatomic molecules are possible if they obey the following selection rules:

$\Delta v = 1$	$\Delta J = +2$	S-branch	
	0	Q-branch	vibrational CARS
	-2	O-branch	
$\Delta v = 0$	$\Delta J = \pm 2$	O-, S-branch	rotational CARS
	0	Q-branch	Rayleigh Scattering

7.2 Coherent Anti-Stokes Raman Scattering

CARS signals are produced by molecules in the strong coherent electric fields of three laser beams. The electric field of two pump beams and a Stokes beam induce a third order polarization in the medium, which is the source of an anti-Stokes wave. The total polarization is given by[26]:

$$\vec{P} = \varepsilon_0 \chi^{(1)} \vec{E} + \varepsilon_0 \chi^{(2)} \vec{E} \times \vec{E} + \varepsilon_0 \chi^{(3)} \vec{E} \times \vec{E} \times \vec{E} \tag{7.5}$$

In this equation $\chi^{(1)}$ represents the normal linear susceptibility which is responsible for diffraction, absorption, Rayleigh- and (spontaneous) Raman scattering. The term with $\chi^{(2)}$ generates hyper Raman scattering and parametric oscillations. In media with inversion

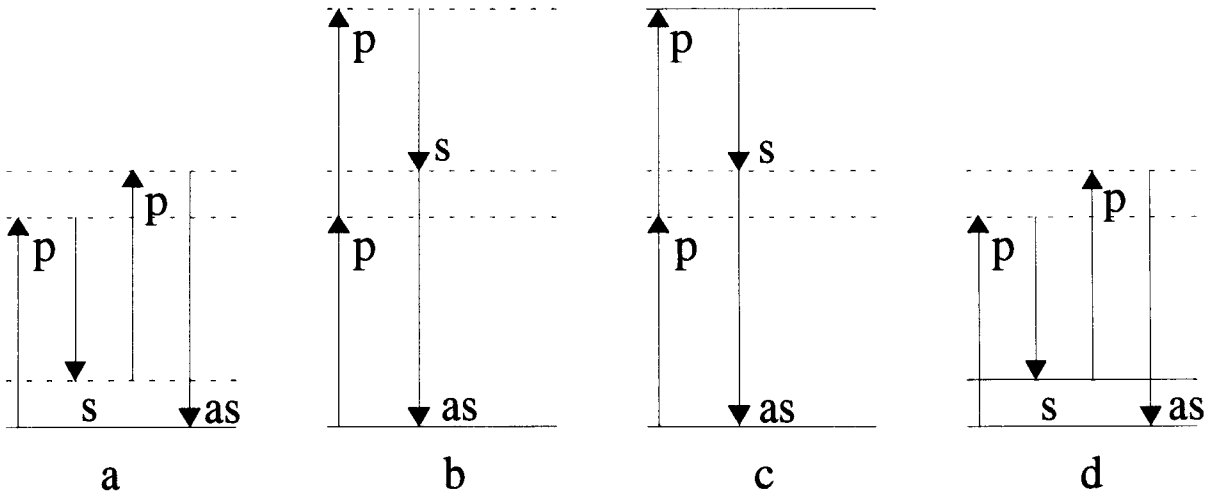

Figure 7.1: Real and virtual (dashed) levels and transitions involved in CARS processes. Cases a and b with transitions between virtual levels contribute to the nonresonant CARS signal. Case c is two photon absorption and of relevance if the upper level is real. The actual CARS process is characterised by case d.

symmetry (like gasses and plasmas) the second order susceptibility vanishes. The lowest order nonlinear effect in a plasma is generated by $\chi^{(3)}$. This third order susceptibility is resposible for third harmonic generation, field induced second harmonic generation, the optical Kerr effect and CARS.

The CARS signal induced by the coherent electric fields of the two pump laser beams and the Stokes beam will be coherent too and behave as a fourth laser beam generated in the medium. This induced laser beam is called the anti-Stokes beam. The frequencies of the laser beams involved follow the relation:

$$2\omega_p - \omega_s = \omega_{as} \tag{7.6}$$

In this equation the subscripts p and s denote the pump and Stokes beam respectively, whereas the subscript as denotes the anti-Stokes beam. Figure 7.1 shows a graphic representation of equation (7.6) in an energy diagram. In the experiments the pump beam has a fixed wavelength. When the Stokes beam is then chosen in such a way that the energy $\hbar(\omega_p-\omega_s)$ matches the energy of a rovibrational transition in a molecular system, $\hbar\omega_{Raman}$, a resonance can be observed. ω_{Raman} is called the Raman frequency or Raman shift:

$$\omega_{Raman} = \omega_p - \omega_s \tag{7.7}$$

This resonance appears as a sudden rise in the intensity of the anti-Stokes beam, I_{as},, which is given by:

$$I_{as} = K\left|\chi^{(3)}\right|^2 I_p^2 I_s \tag{7.8}$$

where K is a proportionality constant, I_p and I_s the pump and Stokes laser intensities. The third order susceptibility $\chi^{(3)}$ can be seen as the sum of a resonant and nonresonant (NR) part:

$$\chi^{(3)} = \chi^{(3)}_{res} + \chi^{(3)}_{NR} \tag{7.9}$$

The nonresonant part is a result of processes a and b in figure 7.1, the resonant part contains all resonant processes like stimulated Raman scattering and CARS. Stimulated Raman scattering is represented by the first two arrows in figure 7.1d. This process will increase the population of the upper level while decreasing the population of the lower level. This effect, saturation, will change the population distribution and therefore affect the rovibrational state

distribution measured with resonant CARS. The presence of saturation can be shown by measuring the dependence of the intensity of the anti-Stokes beam on the background pressure. Equations (7.8) and (7.10) show that the intensity must be proportional to the square of the total number density and therefore to the square of the pressure. Deviations from this relation indicate saturation.

The resonant processes are responsible for the rise in $\chi^{(3)}$ and therefore in the anti-Stokes power when the Raman shift matches a rovibrational transition. For an isolated Q-branch transition the resonant part of the susceptibility (when neglecting stimulated Raman scattering) is given by[9]:

$$\chi_{res}^{(3)} = K' N[\rho(v,J) - \rho(v+1,J)](v+1)\left(1+\frac{1}{6}\frac{J(J+1)}{(2J-1)(2J+3)}\right)\frac{d\sigma}{d\Omega}h(\omega_p - \omega_s) \qquad (7.10)$$

In this equation we can easily see that the CARS nonlinear susceptibility is proportional to the difference of the population factors ρ. Here $\rho(v,J)$ is the probability of occupation of the state with rovibrational quantum numbers v and J(the lower state of the measured Raman transition) and $\rho(v+1,J)$ that of the upper state. $d\sigma/d\Omega$ is the differential Raman-scattering cross section for the $v = 0 \rightarrow 1$ transition, whereas $v+1$ and the following factor between parentheses account for the rise in cross section as a function of lower-state vibrational and rotational quantum numbers. K' is a proportionality constant and N the total number density. For H_2 the distribution of rotational states within one vibrational band is assumed to be in Boltzmann equilibrium at the translational temperature T[27]. For the vibrational state population distribution, however, this is not true. The population factor can then be written as:

$$\rho(v,J) = f(v)g_v(J)/Q_v \qquad (7.11)$$

with $f(v)$ the vibrational population fraction in state v, $g_v(J)$ the rotational population fraction and Q_v the rotational partition function within state v, which can be written as the sum of all rotational population factors in the considered vibrational state:

$$Q_v = \sum_{J=0}^{\infty} g_v(J) \qquad (7.12)$$

The rotational population fraction is given by:

$$g_v(J) = g_J(2J+1)\exp\left(\frac{-E_v(J)}{kT}\right) \qquad (7.13)$$

with $E_v(J)$ the rotational energy of rovibrational state (v, J), and g_J the nuclear spin factor. in H_2 these spin factors are:

$g_J = 1$ for J even,
$g_J = 3$ for J odd

In our experiments we only considered Q-branch transitions for which $\Delta v = 1$ and $\Delta J = 0$. Therefore, combining equations (7.8) to (7.13), we can conclude that the difference in rotational population between two consequtive vibrational levels can be calculated from the square root of the intensity of the anti-Stokes beam, I_{as}, and $\sqrt{I_{as}} / g_J(2J+1)$ should reflect a distribution according to a Boltzmann equilibrium.

Besides proper matching of frequencies due to energy conservation, which results in equations (7.6) and (7.7), conservation of momentum requires a proper matching of $\vec{k}$-vectors. This is necessary for efficient coherent growth of the generated anti-Stokes wave. The matching of

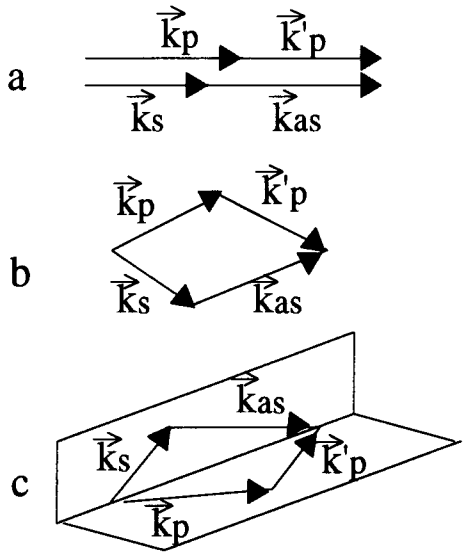

Figure 7.2: Typical momentum matching geometies a) collinear CARS, b) planar BOXCARS and c) folded BOXCARS.

$\vec{k}$-vectors, and focussing, is a good means of controlling the longitudinal spatial resolution of the CARS generation volume[26].
Some typical CARS geometries which satisfy these requirements are (figure 7.2):

1. Collinear CARS, which generates high signal levels but lacks spatial resolution and will induce nonresonant CARS signals in a large volume of gas, windows etc. Focussed collinear CARS, with short focal length lenses, has an improved spatial resolution.
2. BOXCARS, applicable in a planar or folded geometry, has better spatial resolution. This geometry, however, results in lower signal levels and therefore higher detection limits (approximately one order of magnitude[27]).

The preliminary experiments for testing the experimental set-up and software discussed in the next chapter are measured using the collinear CARS geometry. BOXCARS experiments with better spatial resolution will be performed in the future.

8 The experimental set-up

Figure 8.1 shows a schematic view of the set-up as it is used for the CARS measurements (the optical components are listed in table A1 in appendix A). The pumplaser beam is generated by a Spectra Physics GCR 230 50 Hz Nd:YAG laser with a power of 300 mJ per pulse at 532 nm. This Nd:YAG laser also pumps a Spectra Physics PDL3 pulsed dye laser to generate the Stokes beam. The green pump beam and red Stokes beam are put together by a beamcombining mirror for maximum overlap (for collinear CARS) and sent to the plasma vessel. Inside the vessel the third beam (the blue anti-Stokesbeam) will be generated along the mutual axis of the pump and Stokes beam. On the other side of the vessel the green and red laser beams are blocked by several filters, leaving mainly the anti-Stokes beam to travel towards the Hilger-Engis Monospek 1000 monochromator. After wavelength selection the intensity is measured with a Hamamatsu R268 photomultiplier tube (PMT) with a tapered bleeder voltage divider circuit (figure A1 in appendix A). Ten percent of the combined pump/Stokes beam is split off before entering the vessel and is directed through a reference cell containing Argon gas. This reference path has a monochromator and PMT similar to the CARS signal path. The signal from both PMT's is transferred to a PC via a LeCroy 2249A ADC and a Hytec 1330 PC Camac interface.
In the reference cell a nonresonant CARS signal is generated which will have the same dependence on the pump and Stokes laser power as the (non)resonant CARS signal from the vessel (equation (7.8)). Therefore dividing the CARS signal of interest by the reference signal will eliminate the effect of fluctuations in laser power or overlap.
The PC 486 is used for data acquisition and storage and to synchronically scan the Stokes laser and both monochromators (the wavelengths of which are coupled and can be found from equation (7.6)). A computer program was written in order to perform experiments in which the Stokes wavelength is scanned past several rovibrational transitions while simultaneously adjusting the monochromators. More details about the program can be found in the manual in appendix B.

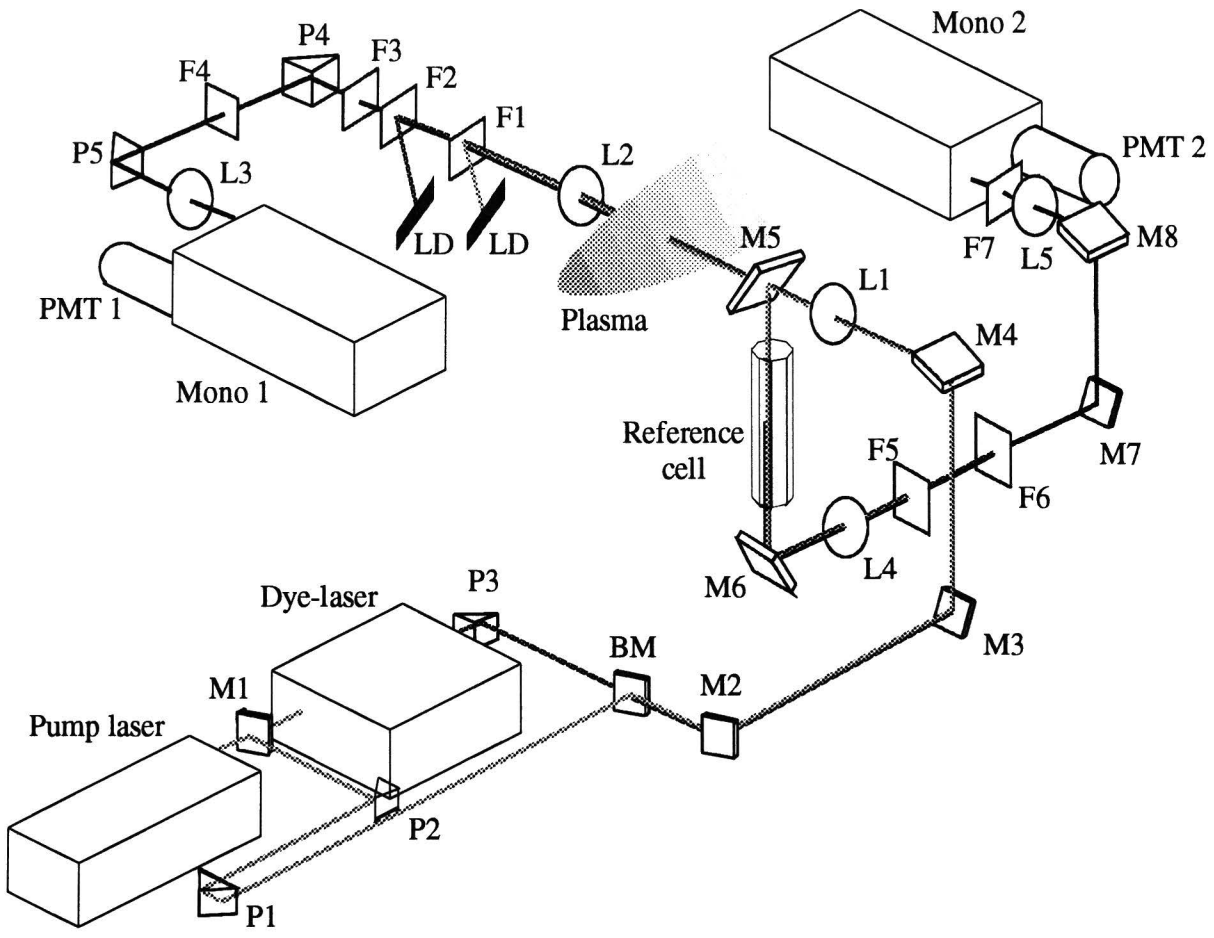

Figure 8.1: Schematic view of the CARS diagnostic. M = mirror, BM = beam-combining mirror, P = prism, L = Lens, F = filter, LD = laser dump and Mono stands for monochromator. The Nd:YAG laser sends 30 % of its power to the dye laser through the beamsplitting mirror M1. Beam-combining mirror BM is used to project the pump and Stokes laser beams onto eachother (for collinear CARS). Lens L1 focusses the beams onto the plasma and argon gas in the reference cell. Several filters are used to only let the anti-Stokes signal enter the monochromators. Details on the optical components can be found in table A1 in appendix A.

9 Experiments and conclusions

9.1 Tests of the diagnostic

The measurements mentioned in this report served as tests to make sure the experimental set-up was working as desired. After several bench-tests of the computer program it was believed to be mostly bug-free and the CARS set-up could be tested. These tests are listed below. Numerical results are listed in appendix A.

1. The wavelength displays of the dye laser and monochromators were checked in order to be able to always select the exact wavelength. The deviations proved to be small (on the order of tenths of percents) and are accounted for in the computer program which controls the wavelength of the dye laser and both monochromators.
2. The linearity of the LeCroy 2249A ADC was tested and proved to be good on the full range of the ADC.
3. The linearity of the Hamamatsu R268 PMT was checked and proved to be extremely bad. Therefore a tapered bleeder voltage divider network (figure A1 in appendix A) was installed which improved the linearity of the PMT. With the new voltage divider circuit the PMT can be used up to 25% of the full ADC range. Other PMT tubes are ordered for future experiments in order to further increase the dynamic range of the diagnostic.
4. The size of the CARS generation volume was measured by measuring the strong (relative to the surrounding gas) nonresonant CARS signal of a 1 mm thick glass plate at several positions near the focal point of the lenses. The full 1/e width of the CARS generation volume was measured to be 52 mm (figure A3 in appendix A).

The reference leg of the set-up was still under construction during the experiments discussed in the next paragraph. This means that the detection limit and signal to noise ratio will be improved in future experiments.

9.2 Collinear CARS; the first results

Once the CARS diagnosic was operational the first spectra of rovibrational lines could be measured. The size of the generation volume was known to be 52 mm. In order to avoid measuring too much surrounding gas instead of plasma the measurements were performed at 70 mm from the nozzle of the arc. In this region, just behind the stationary shock, the plasma expansion is large enough to contain the whole CARS generation volume.

These measurements are shown in figure 9.1. The top graph shows the CARS measurements of rotational levels in the $v = 0 \rightarrow 1$ Q-branch transitions of 0.53 Torr H_2 at room temperature. When compared to the lower graphs it is obvious that not as many rotational levels are occupied as in the plasma. This is a result of the fact that the (rotational) temperature is lower in the gas. All measurements in the plasma clearly show the effect of the different nuclear spin factor for even and odd J values. The higher intensity for odd levels stems from the fact that g_J is 3 for odd J and only 1 for even J. Figure 9.2 shows the rotational lines of $v = 0 \rightarrow 1$ and $v = 1 \rightarrow 2$ transitions, thus showing that the expectation of measuring vibrational transition from $v = 1$ to 2 is fulfilled.

Figure 9.3 shows Boltzmann plots for the measurements shown in figure 9.1. In these plots the slope of the (fitted) drawn lines is inversely proportional to the rotational temperature. Since

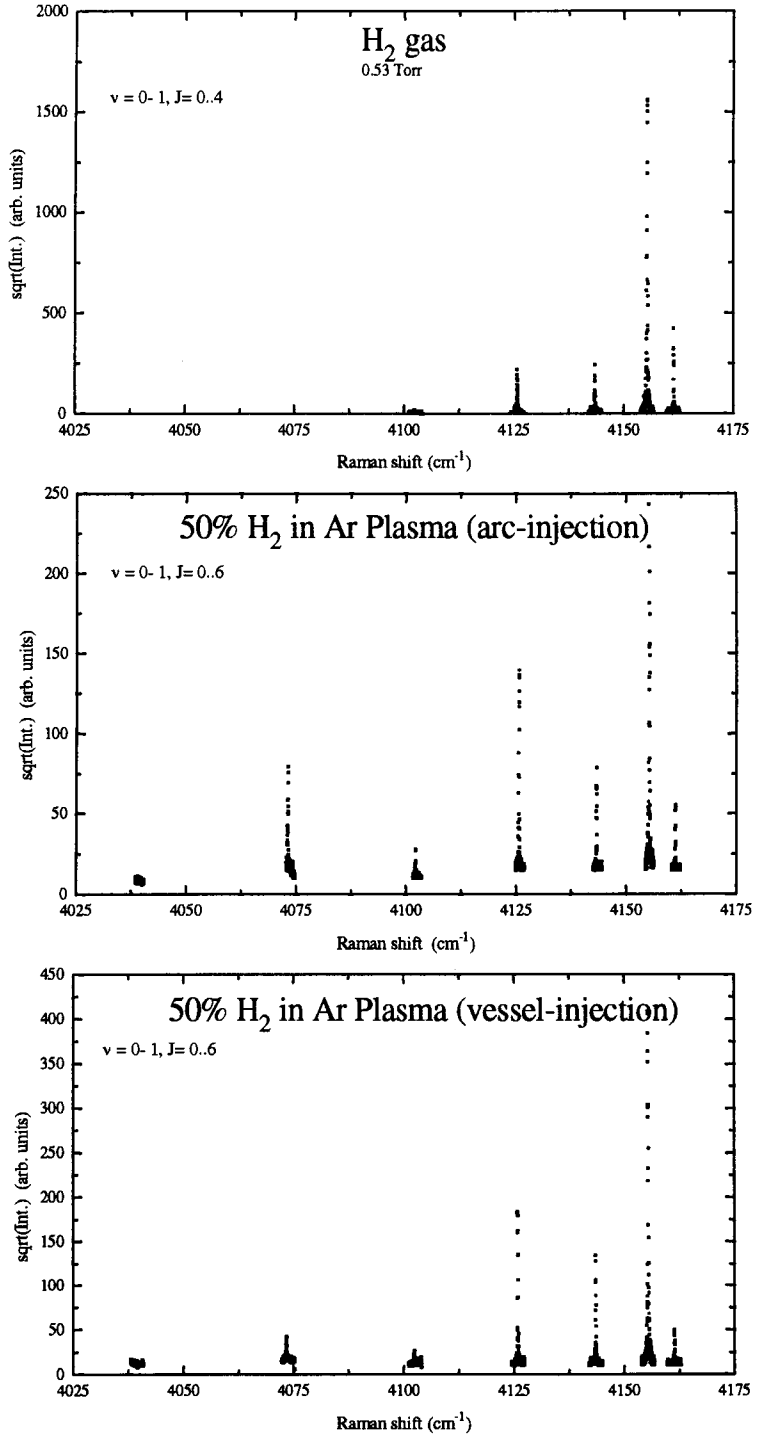

Figure 9.1: Rovibrational transitions obtained from collinear CARS measurements. From left to right the rotational quantum number J decreases. The top graph shows the measurements of hydrogen gas, the lower two graphs for a plasma. The plasma conditions are: pressure = 0.70 Torr, total gas flow = 3.5 slm and the current through the arc = 50 A. All measurements were performed at a distance of 70 mm from the nozzle.

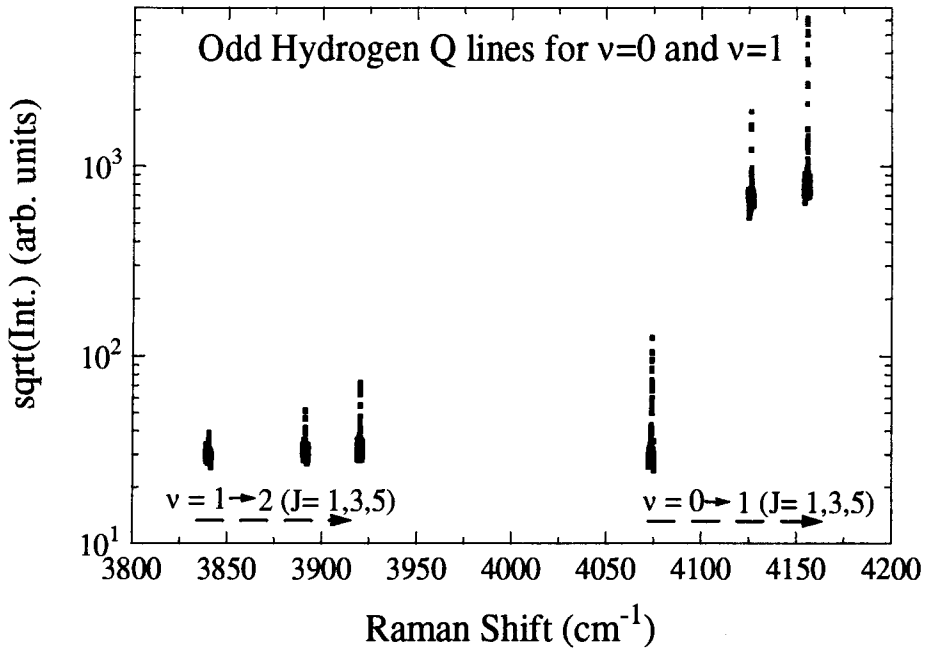

Figure 9.2: Collinear CARS measurements on 50% H_2 plasma, at 1.0 Torr, 3.5 slm, 55A and 20 mm from the nozzle. In this experiment only the stronger odd lines are measured. The $v = 1 \rightarrow 2$ rotational lines can be clearly observed. From left to right the rotational quantum number J decreases.

the rotational state distribution within one vibrational band in H_2 will resemble a Boltzmann distribution[9] the densities divided by their statistical weight, $N/g_J(2J+1)$, of the rotational states will lie on a straight line when plotted logarithmically versus the rotational energy. The first plot of figure 9.3 shows that the measured rotational temperature in the 0.53 Torr H_2 gas is very close to room temperature. This is as could be expected since it is reasonable to assume that the rotational temperature is in equilibrium with the translational (kinetic) temperature[27]. The rotational temperatures measured in the plasma clearly show two temperatures. This is most likely due to the fact that with collinear CARS the H_2 density is measured in a section of the vessel. Therefore the measurement will contain information about the plasma and the surrounding (relatively cold) gas. The fact that during the experiments the focus of the laser beams was, erroneously, not in the plasma but in front of it will increase this effect since in this case more 'cold gas' is measured than in the case of the focus exactly in the middle of the plasma. The higher temperature, obtained from the higher lying v= 4,5,6 levels, corresponds to the rotational temperature in the plasma, since the higher rotational levels are expected to be more abundant in the plasma region. The lower temperature, obtained from the lower rotational states, corresponds to an average temperature of the plasma and the surrounding gas since these lower rotational levels will be present in the surrounding gas as well as in the plasma. This effect, caused by poor spatial resolution, is well known in CARS and can be diminished by the use of BOXCARS which improves spatial resolution substantially.

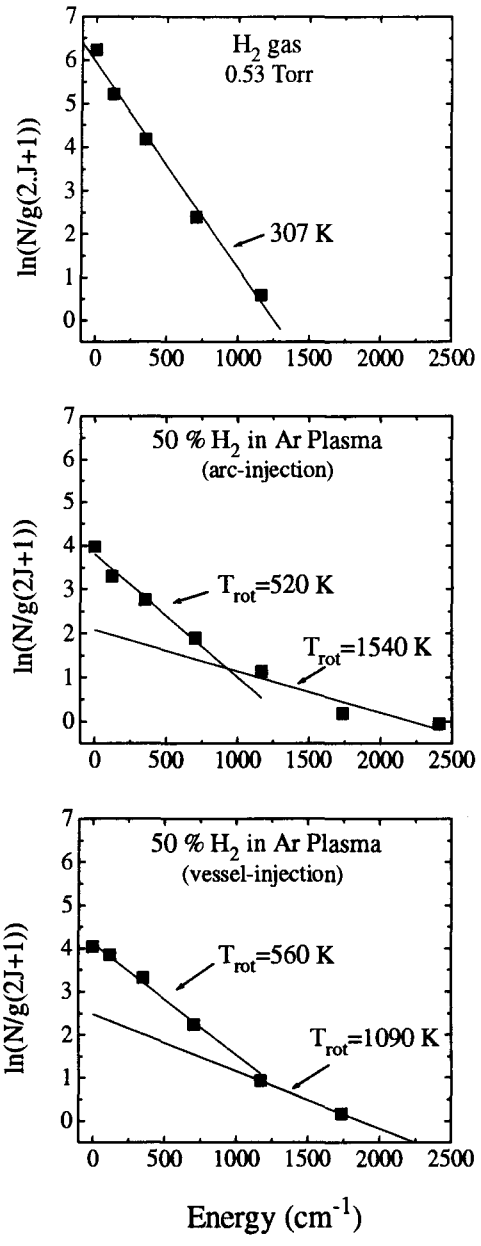

Figure 9.3: Boltzmann plots of the CARS measurements. The slope of the drawn lines is inversely proportional to the rotational temperature. The measured rotational temperature in the H_2 gas is very close to room temperature. The rotational temperatures measured in the plasma clearly show two temperatures. This is most likely due to the fact that with collinear CARS the H_2 density is measured in a long section of the vessel. Therefore the measurement will contain information about the plasma and the surrounding (relatively cold) gas. The fact that the focus of the laser beams was not in the plasma but in front of it during the experiments will increase this effect.

9.3 Conclusions

The measurements indicate that the program written for performing computer controlled experiments is able to accurately position the dye-laser and monochromators. All components of the diagnostic are tested for deviations of ideal behaviour. The error in the displayed wavelengths of both the laser and monochromators is accounted for in the program. The

electronic detection branch is tested for linearity and proved to be linear for 25% of the full ADC range.
The preliminary CARS experiments showed that differences in population of rotational levels between the $v = 0$ and 1 and $v = 1$ and 2 vibrational states can be measured. The mesasurements of rotational lines of the $v = 0 \rightarrow 1$ transition also yielded rotational temperatures. The measured rotational temperature of 0.53 Torr of H_2 gas proved to be in good agreement with the known value (room temperature). The measurements in the plasma showed two different rotational temperatures for the higher and the lower rotational states. This is probably due to the fact that the CARS generating volume contains both plasma and surrounding gas when using the collinear geometry.

9.4 Recommendations

For future experiments it is important to increase the dynamic range of the diagnostic by exchanging the R268 photomultiplier tubes with an other type which is more suited for measuring pulsed signals with high peak values.
The installation of the reference cell will decrease the detection limit (currently approximately 10^{19} m^{-3}) by approximately an order of magnitude. This will allow for more accurate measurements of the higher, less populated, rotational states. Measuring higher vibrational levels will also be one of the possibilities.
The introduction of BOXCARS will improve the spatial resolution of the CARS measurements (although it increases the detection limit by approximately a factor of 10). Better Spatial resolution will decrease the effect of surrounding gas on the measurements. Increasing laser power or beam diameter can possibly compensate for the weaker signals which result from the smaller CARS generation volume.
A special computer program for calculating the densities of rovibrational levels, which is currently being written by Jacobs[28], will decrease the time needed for these calculations, thus increasing the rate at which CARS measurements can be performed and processed in the future.

Acknowledgements

Here I would like to thank all who have made it possible for me to graduate at the Eindhoven University of Technology. Some by making things easier some harder:

Ralph Meulenbroeks, Richard Engeln, Marc Beurskens, Jan Snoeijer, Richard van de Sanden, Joost van der Mullen, Daan Schram, Herman de Jong, John Gielen, Bertus Hüsken, René Severens, Bart van der Sijde, Jeanne Loonen, Ries van de Sande, Hans de Regt, Roger Paffen, Jeroen Jonkers, Zhou Qing, Mark de Graaf, Danny Benoy, Isa de Bari, Frank Umans, Leon Jacobs, Leo van IJzendoorn, Martien de Voigt, Jeff Harris, Martin Williams, Tadaaki Kaneko, Omar Nagi, Paul Koenraad, Joachim Wolter, Else van Eyndhoven, Fons de Waele, Wim de Jonge, Frans Blom, Austin Bruil, Frits de Hoog, Rob van Welzenis, Coen Swüste, Johan van de Heide, Marijne Gelten, Klaas Kopinga, Herman Beijerinck, Henk Hagedoorn, Andries Sarlemijn, Frans Sluyter, Wim de Muynck, Jan Millenaar, Gerrit Kroessen, Mico Hirschberg, Bob Tolsma, Herbert Gijsman, Carel Massen, Jan Voskamp, Onno Rademaker, Piet Schram, Boudewijn Verhaar, Wim van Haeringen, Gert-Jan van Heijst, Ad Houtsma, Frans Blommaert, Armin Kohlrausch, Marius Bogers, Kees Box, Toos Box, Nina Box, Curt van de Cruijs, Ted van Maanen, Rob Gijsbers, Gert-Jan van Vonderen, David van Lith, Thijs Bressers, Jurgen Smits, Stefan Slenders, Ger Smolders, Ludwig Boltzmann, Megh Saha, George Stokes, Chandrasekhara Raman, Johann Balmer, Joseph Thomson, John Strutt, Max Planck, Albert Einstein, Jimi Hendrix, Leo Fender, Rory Galagher, Seth Lover, Lester Polfus, Richard Janssen, Robin Berlijn, Herman Deinum, Wouter Planteydt...
And of course everyone who feels he or she should be on this list but isn't.

Literature References

[1] Polytechnisch weekblad, no. 33/34, year 23, august 13 1992.

[2] A.T.M. Wilbers,
Thesis, Eindhoven University of Technology, january 1991.

[3] M.C.M. van de Sanden,
Thesis, Eindhoven University of Technology, december 1991.

[4] A.J.G Helvoort,
Internal report, VDF/NT 92-11, Eindhoven University of Technology, may 1992.

[5] E. van de Ven,
Graduation report, VDF/NT 93-17, Eindhoven University of Technology, august 1993.

[6] A.J. van Beek,
Internal report, VDF/NT 93-04, Eindhoven University of Technology, january 1993.

[7] R.F.G. Meulenbroeks, P.A.A. van der Heijden, M.C.M. van de Sanden and D.C. Schram,
J. Appl. Phys. **75** (6), 2775 (1994).

[8] A.J. Snoeijer,
Graduation report, VDF/NT 94-13, Eindhoven University of Technology, august 1994.

[9] M. Péalat, J.P.E. Taran and J. Taillet,
J. Appl. Phys. **52** (4), 2687 (1981).

[10] J.J.A.M. van der Mullen,
Thesis, Eindhoven University of Technology, 1986.

[11] R.F.G. Meulenbroeks, A.J. van Beek, A.J.G. Helvoort, M.C.M. van de Sanden and D.C. Schram,
Phys. Rev. E **49** (5), 4497 (1994).

[12] H.W. Drawin and P. FehlenBock,
Data for plasmas in local thermodynamic equilibrium, Gauthier-Villars, Paris, 1965.

[13] B. van der Sijde,
Inleiding Plasmafysica, Lecture Notes 3461, Eindhoven University of Technology, february 1992.

[14] R. Paffen,
Graduation report, VDF/NT 93-19, Eindhoven University of Technology, october 1993.

[15] M.N.A. Beurskens,
Graduation report, VDF/NT 94-14, Eindhoven University of Technology, august 1994.

[16] M.C.M. van de Sanden, J.M. de Regt and D.C. Schram,
Phys. Rev. E **47** (4), 2792 (1993).

[17] M.J. de Graaf, R. Severens, R.P. Dahiya, M.C.M. van de Sanden and D.C. Schram,
Phys. Rev. E **48** (3), 2098 (1993).

[18] B. Jackson and M. Persson,
J. Chem. Phys. **96** (3), 2378 (1992).

[19] R.D. Smith and J.H. Futrell,
Int. J. of Mass Spectr. and Ion Phys. **20**, 33 (1976).

[20] A.B. Rakshit and P. Warneck,
J. Chem. Phys. **74** (5), 2853 (1981).

[21] I. de Bari,
Internal report VDF/NT 94-19, Eindhoven University of Technology, september 1994.
[22] T.E. Sharp,
Atomic Data **2**, 119 (1971).
[23] D.M. Hirst et al.
Mol. Phys. **77** (2), 279 (1992).
[24] P.W. Atkins,
Molecular Quantum Mechanics, second edition, Oxford University Press, 1983.
[25] K.P. Huber and G. Herzberg,
Molecular Spectra and Molecular Structure, IV: Constants of diatomic molecules.
Van Nostrand Reinhold Company, 1978.
[26] T. Doerk, J. Ehlbech, P. Jauernik, H. Kempkens and J. Uhlenbusch,
Lecture given at the VI International School on Quantum Electronics-Laser-Physics and Applications, Varna (Bulgaria), september 1990.
[27] M. Péalat, J.P.E Taran, M. Bacal and F. Hollion,
J. Chem. Phys. **82** (11), 4943 (1985).
[28] L. Jacobs,
Internal report, Eindhoven University of Technology, to be published.

Appendix A

CARS equipment

Dye-laser
The Spectra Pysics PDL3 Pulsed Dye Laser was checked for nonlinear diplay of wavelengths. It was found that the wavelength was given by:

$$\lambda_{Display} = 4\times(-18.725 + 1.004\cdot\lambda_{True})$$

where the factor 4 stems from the fact that the grating is used in fourth order. This deviation is accounted for in the computer program.
The dye laser was initially operated with a LDS 698 dye which has an efficiency peak for the $v = 0 \rightarrow 1$ transition. An other dye, DCM, was planned for use in measurements $v \approx 2, 3$. Difficulties to find vibrational transitions from $v = 1$ to 2, however, inspired to use a mixture of both dies to get a more even efficiency over the whole spectral range.

Monochromators
Both Hilger-Engis Monospek 1000 monochromators were checked for errors in the displayed wavelength. This was done by measuring and identifying emission lines of a low pressure Ar lamp in the region of interest. The displayed wavelengths are given by:

Signal : $\lambda_{Display} = 1.5\times(-0.49383 + 1.00159\cdot\lambda_{True})$
Reference : $\lambda_{Display} = 1.5\times(0.19834 + 1.00023\cdot\lambda_{True})$

The factor 1.5 is a result of the use of a grating with 1800 grooves/mm. These deviations were accounted for in the computer program which steps the monochromators.

Photomultipliers
For the experiments two Hamamatsu R268 photomultiplier tubes were used The linearity of these PMT's however left a lot to be desired. Correspondence with the manufacturer learned that this was a common problem when using this type of tubes in experiments with pulsed sources. This led to ordering new tubes which will be installed for future experiments. In the mean time a tapered bleeder voltage divider network (smaller voltage difference between first dynodes and larger between last dynodes) was installed (figure A1) to obtain better linearity.

Anolog to Digital Converter
The LeCroy 2249A ADC, which integrates the charge (current) produced by the PMT's, was also checked for linearity by feeding the input of the ADC with a known variable current and measuring the output signal with the PC (through the Hytec 1330 PC Camac interface). The results are shown in figure A2 which shows good linearity over the range of 0 to 1.8 mA.

Dynamic Range
Since the ADC proved to be linear over the full range the limit of maximum dynamic range of the diagnostic is determined by the PMT. The nonlinearity of the photomultiplier tubes dictates a maximum dynamic range of 25% of the full ADC scale, in this region the diagnostic as a whole will behave as a linear system.

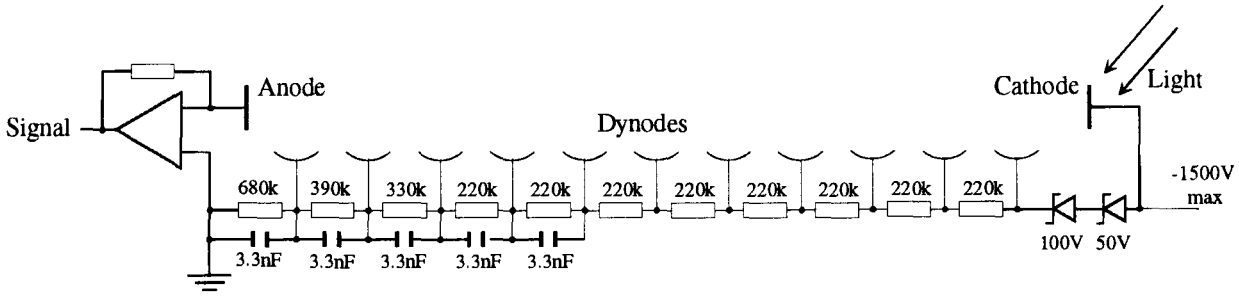

Figure A1: Tapered bleeder voltage divider circuit for the Hamamatsu R268 PMT. The voltage between the last dynodes (and the anode) is increased (not the usual linear distribution of voltage over the dynodes) for more amplification in the last stages. The capacitors are to make sure no saturation effects occur in the last stages (enough electrons to produce the current avalanches).

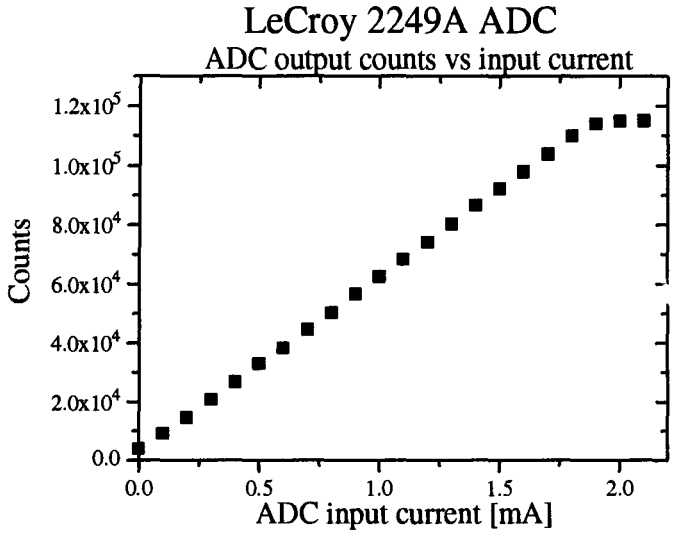

Figure A2: ADC output in counts as a function of input current (ADC samples 100 ns at 50 Hz) each point is the mean of five measurements of 100 shots.

Table A1: List of optical components of the CARS diagnostic.

Comp.	Description	Comp.	Description
BM	beam-combining mirror	F1,5 F2,6 F3,4,7	interference filter (blocks green) Low pass filter (blocks red) Band pass filter (lets blue pass)
M1 M2,3,4, 6,7,8 M5	30/70 beam splitter broadband reflector quartz plate (= 90/10 beam splitter if positioned at 45°)	P1-5	prisms
L1,2,4 L3,5	f= 1000 mm quartz lens f= 150 mm lens		

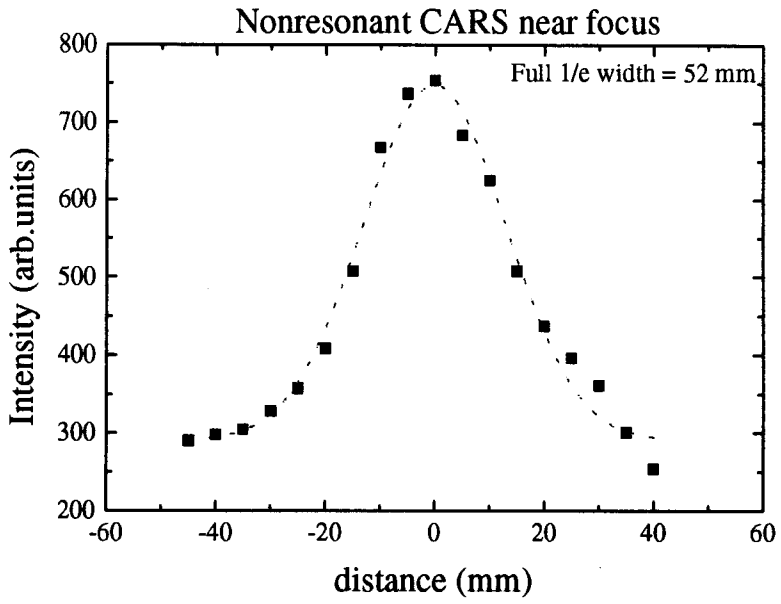

Figure A3: Measurement of nonresonant CARS in a 1 mm thick glass plate as a function of distance to the focal point of the quartz lens. The dashed curve represents a Gaussian fit which yields the 1/e width of the CARS generation volume. This width is 52 mm.

Appendix B: Manual to the CARS program

Contents

1 Program manual

1.1 The menus

The program for measuring CARS signals is based on Turbo Vision (from version 6.0) example programs to obtain a menu controlled userinterface. The main menu, which appears on the screen when the program is started, contains five submenus. Each submenu again has some items to choose from. The total menu has the following format:

File	Info	Plot	Laser	Options
Exit	Command	Plot File	Set Home F8	Test Mode
	H2 Spectrum	On line	Go Home F9	View Camac
			Go To	----------
			----------	Hydrogen Spectrum
			Scan	

These submenus have the following functions:

Info: The information menu has two items: *Command* shows a review of the submenus *Laser*, *Plot* and *Options* on the screen. *H2 Spectrum* gives a table of rovibrational hydrogen lines with their quantumnumbers, Ramanshifts and the corresponding wavenumber for the dye laser.

Plot: The *Plot File* item asks for a file to be plotted on the screen, *On Line* shows a toggle switch. When chosing 'off ', the data will be written to the screen as numbers, with *On Line* active (on) the data will be shown in numbers as well as in a plot.

Laser: This is the basic control menu for the dye laser and both monochromators. With *Set Home* the laser and monochromators can be initialised and synchronised, thus getting the experimental set-up prepared for measurements. The signal monochromator is referred to as *Mono 1*, the reference monochromator as *Mono 2*. The laser will automatically go to the home position (the monochromators will follow any step made by the laser) which will be stored and can be retrieved with the command *Go Home*. The *Program* command will bring up a window for entering measurement parameters like start and stop Raman shifts, stepsize, name of datafile etc. Upon pushing the OK button the laser will be sent to the start position of the measurement and the experiment will be carried out automatically. *Go To* allows to set the laser and both monochromators at a certain position (usually a certain line to optimize laser and monochromator position by hand).

Options: The special options are *Test Mode*, which allows to turn the laser and monochromators off, and to choose between straight counts or data devided by the reference signal, *View Camac*, which shows the signal of the photomultipliers without scanning, and *Hydrogen Spectrum*. This last option will show a matrix in which pre-programmed rovibrational hydrogen lines can be chosen to be measured allowing a quick stepping through the spectrum and only measure lines you are interested in. This option starts the experiment upon OK.

1.2 How to use the program

This section gives a short recipe for performing CARS experiments with the CARS program.

Important: Always start a session with *Set Home* to make sure that the laser and both monochromators are synchronised. It recommended to enter a hydrogen line for home position and to optimise the position of the laser and monochromator by hand. In this case the program believes it set the right positions, it won't harm to make that true.

Starting a session:

1. *Laser→Set Home.* Enter the right values, remember signal comes from mono 1 and reference from mono 2. Is the home position entered in counter readings or cm^{-1} ?
2. *Options→Test Mode.* Chose divided or straight data.
3. *Plot→On Line.* Chose on line graphics on/off.

Making a scan:

- *Laser→Scan.* Enter a start Raman Shift that is higher than the stop position, this way the laser and monos don't correct for backlash* every step they make. This saves time. Enter the name of the datafile and go.

Scanning hydrogen lines:

- *Options→Hydrogen Spectrum.* Select the right v and J values and enter the other parameters.

To **stop a measurement** while it is **not finished** just press **F1**, the datafile will be saved and the program returns to the main menu. The laser will automatically return to the home position.

* Backlash is a small free movement the stepper motor can make without affecting the mechanism which changes the wavelength (both for monochromator and dye laser). This introduces a possible error in the wavelength. By taking care the last movement of the stepper motor is always in the same direction (this is the backlash correction), the error made by the free movement is the same for each step. This only introduces a small, systematic, error in the wavelength.

2 The program

2.1 The program layout

In figure B2.1 a schematic of the program layout is shown. In this schematic the different layers

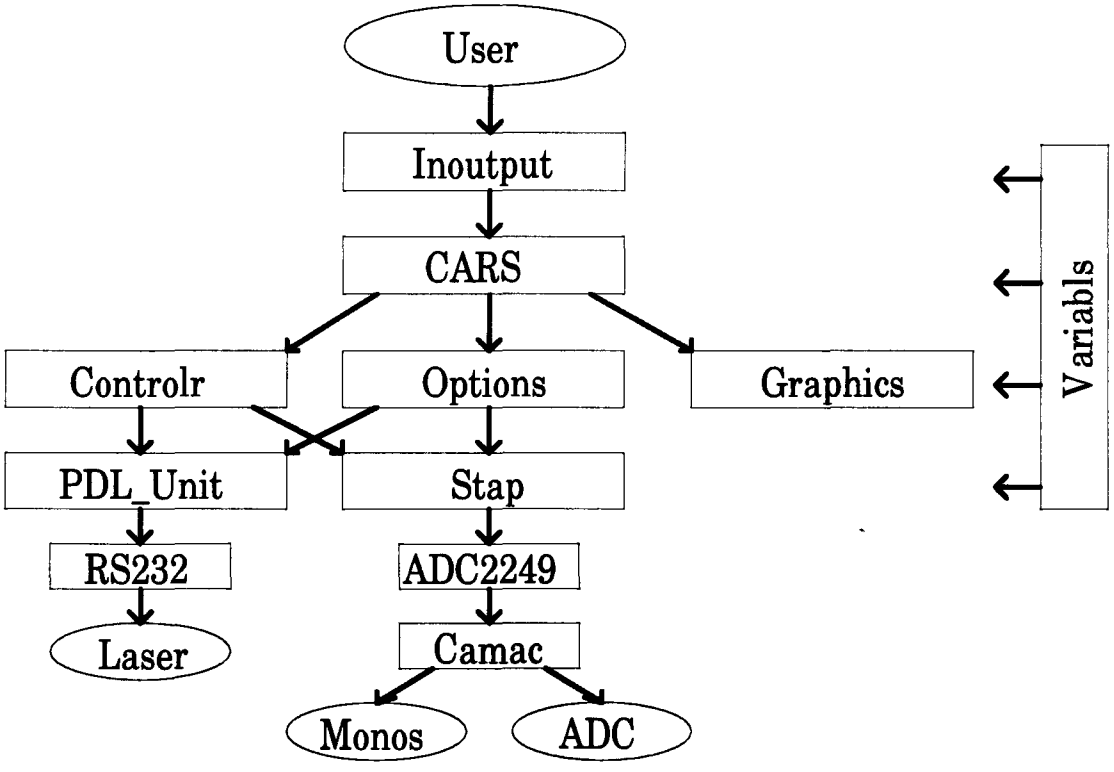

Figure B2.1: Schematic of the layout of the measuring program.

of the program are shown. On the top is the user, who only interacts with the program via the windows created by the *Inoutput* unit. This unit sets parameters and gives the orders to use other units or procedures. *CARS* is the main program. The only task of *CARS* is to receive the orders from *Inoutput* and to activate the procedures necessary to carry out these orders. The third layer of the program is split in three. The two main units are *Controlr*, which contains all the procedures needed for the Laser submenu, and *Options*, which contains all procedures for the Options submenu. These units contain the counters which store the position of the dye laser and the monochromators. *Graphics* contains procedures for plotting a file onto the screen. The forth layer is split in two: *PDL_Unit* contains all procedures for initialising and stepping the laser, *Stap* contains all procedures for stepping the monos and reading the ADC. Layer five and six of the program are the interface with the experimental hardware. There is one overall unit, *Variabls*, which contains all variabels needed in the four main layers of the program. In paragraph 2.3 the units, and their procedures, will be discussed in more detail.

2.2 The position counters

Before discussing the separate procedures, the variabels which store the position of the laser and the monochromators are explained.

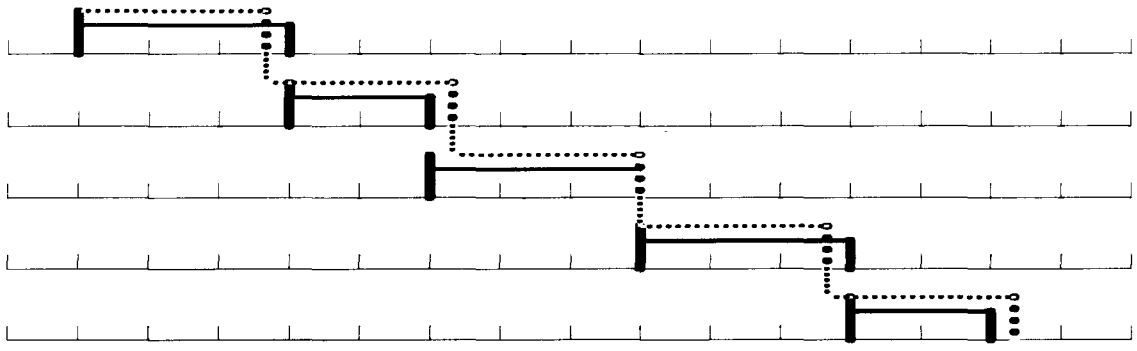

Figure B2.2: Schematic of the calculation of the position by the various counters. Each horizontal line represents a consecutive step. The dotted lines represent the accurately calculated position at which the laser should be positioned (wavel (times a constant factor)). The drawn lines are the approximated positions (count) which coincide with single steps of the stepper motor (the small vertical lines on the axes). The calculation of the position of the monochromator is done in a similar way.

For the experiments it is most efficient to give the position of the laser and monos in wavenumbers [cm^{-1}], for the control of the laser and monos however wavelengths [Å] are required. The experiment also ask for positions in real numbers whereas the use of a stepper motor implies that the position is given in an integral number of motorsteps.
In order to get an accurate representation of the positions several variabels are needed:

pos (current*pos*, home*pos* etc.): The wavenumber of the dye laser in cm^{-1}.

wavel: The wavelength of the dye laser in Å (represented as a real).

count: The single motor step closest to the desired wavelength of the dye laser (represented as an integer).

The values for the laser position, as entered in the windows (in cm^{-1}, *pos*), will be converted to Å (*wavel*) by the procedure *convert*. When stepping, the program will calculate every next position, i.e. where the laser should be positioned, using *wavel* as counter (to prevent an accumulation of round off errors)(see figure B2.2). Since the position of the laser in motorunits is stored, the program always knows the exact position in these motorunits, and therefore can always calculate the number of steps the motor has to make to position the laser as close to the desired new position (*wavel*) as possible. The position of the monochromators (*monopos*, in motorunits) is calculated from the exact position of the laser (i.e. in motorunits) in order to optimise the match between dye laser and monochromator wavelength.

2.3 Units and procedures

In this Paragraph the procedures from the units *Controlr*, *Options* and *Graphics* are summed with a short explanation of their purpose and what they do.

Controlr:

Setlaserstart: This procedure calculates the number of steps the laser (steps_l) and both monochromators (steps_m) (already synchronised!) have to make to get from the current position to the entered desired position, steps the laser and monos to this position and updates *currentcount*, the actual position of the laser.

Steplaser: Tells the laser and monos to make one step of the size *stepsize* as entered in the window *Program* or *Hydrogen Spectrum* (and converted from cm^{-1} to Å (*pos* to *wavel*) by *Convert*), after having calculated the number of motorsteps for the dye laser and monos corresponding to stepsize in cm^{-1}.
Sendhome: Recovers the homeposition,as entered in the window *Set Home*, from the memory, calculates the number of motorsteps to be made and sets the laser and both monochromators at the home position.
Buildhome: From the entered positions of the laser and both monos separately, and from the newly entered homeposition this procedure calculates and sets the laser at the right homeposition. The monochromators are both set at exactly the same wavelength corresponding to the home position of the laser (taking into account their individual deviation of the displayed wavelength (i.e.the monofactor, for calculating the number of motorunits, is different for both monos)).
Convert: converts the entered wavenumbers [cm^{-1}] (*pos*) to wavelengths [Å] (*wavel*) and calculates the stepsize in Å (constant steps in cm^{-1} imply variable steps in Å).
Meten: creates datafile, tells laser and monos to make steps until the stopposition is reached and gives the order to read the ADC after each step (procedure *get_cars_data*), writing the result to the datafile. This procedure also writes the data to the screen in CRT mode, when no on line graphics are selected, or in the graphics mode, when 'On Line' is on, displaying the CARS signal as white dots and the reference signal as red dots. In this case it also calculates the axis labels for the *Drawframe* procedure in *Options*. If requested the laser and monos will be sent to the homeposition after the measurement has finished.

Options:
JumpH2spectrum: finds out which v, J combinations are chosen to be measured (by interpreting the values of *Whichband[J]*) and creates a datafile.
Takeband: calculates the bands around the lines to be measured and tells the laser and monos to step through those bands. After each step the ADC's are read and the results written to the datafile. This procedure also checks wether to display the data on the screen in CRT or graphics mode. In the last case the procedure also calculates labels for the procedure *Drawframe*. When the measurement is finished the laser and monos will be sent to the homeposition.
Viewcamac: reads the ADC's the entered number of times, without stepping the dye laser or the monos and displays the results on the screen.
Drawframe: This procedure draws the frame of the plot when on line graphics are selected. The minimum and maximum values displayed near the axes are calculated in *Takeband* or *Meten*.
Giveinfo: shows selected information files on the screen.
Get_cars_data: reads the ADC's the entered number of times and checks for ADC overshoot. This procedure also throws away data points which deviate from the mean value by a number greater than the standard deviation. Finally the differences in frequency response of both monochromators and PMTs are accounted for.

Graphics:
Graphics: Draws a frame and opens the entered file. From the data minima and maxima for both axes are extracted and the data are plotted as points (*putpixel*) on the screen.